Chapter 10

https://doi.org/10.32685/pub.esp.35.2019.10
Published online 26 September 2019

Fragments of a Permian Arc on the Western Margin of the Neoproterozoic Basement of Colombia

Gabriel RODRÍGUEZ–GARCÍA[1]*, Ana María CORREA–MARTÍNEZ[2], Juan Pablo ZAPATA–VILLADA[3], and Gloria OBANDO–ERAZO[4]

1 grodriguez@sgc.gov.co
Servicio Geológico Colombiano
Dirección de Geociencias Básicas
Grupo de Estudios Geológicos Especiales
Calle 75 n.° 79A–51
Medellín, Colombia

2 amcorrea@sgc.gov.co
Servicio Geológico Colombiano
Dirección de Geociencias Básicas
Grupo de Estudios Geológicos Especiales
Calle 75 n.° 79A–51
Medellín, Colombia

3 jpzapata@sgc.gov.co
Servicio Geológico Colombiano
Dirección de Geociencias Básicas
Grupo de Estudios Geológicos Especiales
Calle 75 n.° 79A–51
Medellín, Colombia

4 gobando@sgc.gov.co
Servicio Geológico Colombiano
Dirección de Geociencias Básicas
Grupo de Estudios Geológicos Especiales
Calle 75 n.° 79A–51
Medellín, Colombia

* Corresponding author

Abstract New petrographic, whole–rock geochemical, and U–Pb–zircon geochronologic data combined with data from previous studies enabled identification of a fragmented Permian magmatic arc with ages ranging from 294 to 260 Ma in the Colombian Andes. The arc is exposed along the southeastern slope of the Central Cordillera towards the Upper Magdalena Valley, serranía de San Lucas, and Sierra Nevada de Santa Marta.

The arc fragments consist of plutons on the western margin of the Neoproterozoic basement and show wide lithological variation in both igneous (monzodiorites, quartz monzonites, tonalites, granodiorites, monzogranites, and syenogranites) and metamorphic (migmatites, gneisses, and mylonitic gneisses) rocks. The granites have a metaluminous to peraluminous character and correspond to calc–alkaline to high–potassium calc–alkaline series formed in a continental arc environment. Some bodies are associated with metamorphic rocks (La Plata Granite and Icarco Complex), which may correspond to the roots of the arc, and others show superimposed dynamic metamorphism (the Nechí Gneiss and El Encanto Orthogneiss). The Permian plutons, unidentified in previous studies because of their lithological similarities to the volume of magmatism that occurred during the Early to Middle Jurassic, are dispersed along with the Neoproterozoic basement. The Permian plutonism that intruded the basement of the northern Andes possibly originated in a subduction zone located on the western margin of Gondwana.

Keywords: *geochemistry, U–Pb geochronology, Colombian Andes, igneous and metamorphic rocks.*

Resumen Nuevos datos de petrografía, geoquímica de roca total y geocronología U–Pb en circón junto con la reinterpretación de datos reportados en trabajos previos permitieron identificar en los Andes colombianos un arco magmático fragmentado con actividad entre 294 y 260 Ma. Este arco está expuesto a lo largo del flanco suroriental de la cordillera Central en el Valle Superior del Magdalena, la serranía de San Lucas y la Sierra Nevada de Santa Marta.

Los fragmentos de arco consisten en plutones localizados en la margen occidental del basamento neoproterozoico y presentan una amplia variación litológica entre ro-

Supplementary Information:

S: https://www.sgc.gov.co/LibroGeologiaColombia/tgc/sgcpubesp35201910s.pdf

Citation: Rodríguez–García, G., Correa–Martínez, A.M., Zapata–Villada, J.P. & Obando–Erazo, G. 2019. Fragments of a Permian arc on the western margin of the Neoproterozoic basement of Colombia. In: Gómez, J. & Mateus–Zabala, D. (editors), The Geology of Colombia, Volume 1 Proterozoic – Paleozoic. Servicio Geológico Colombiano, Publicaciones Geológicas Especiales 35, p. 205–239. Bogotá. https://doi.org/10.32685/pub.esp.35.2019.10

cas ígneas (monzodioritas, cuarzomonzonitas, tonalitas, granodioritas, monzogranitos y sienogranitos) y metamórficas (migmatitas, gneises y gneises miloníticos). Los granitos son de carácter metaluminoso a peraluminoso y corresponden a la serie calcoalcalina a calcoalcalina alta en potasio, formados en un ambiente de arco de margen continental. Algunos cuerpos presentan rocas metamórficas asociadas (Granito de La Plata y Complejo Icarco) que pueden corresponder a las raíces del arco, mientras que otros exhiben metamorfismo dinámico sobreimpuesto (Gneis de Nechí y Ortogneis El Encanto). Los plutones pérmicos están dispersos con el basamento neoproterozoico y no se habían identificado en trabajos anteriores debido a sus similitudes litológicas con el magmatismo que ocurrió durante el Jurásico Temprano a Medio. El plutonismo pérmico que intruye el basamento de los Andes del norte posiblemente se originó en una zona de subducción localizada en la margen occidental de Gondwana.

Palabras clave: *geoquímica, geocronología U–Pb, Andes colombianos, rocas ígneas y metamórficas.*

1. Introduction

Permian age rocks in Colombia have been described in the core of the Central Cordillera, in the serranía de San Lucas and in the Sierra Nevada de Santa Marta, without clear differentiation between metamorphic belts, granitoids, and peraluminous granitic gneisses (Cardona et al., 2010a, 2010b; Cochrane et al., 2014; Leal–Mejía, 2011; Restrepo et al., 2011; Spikings et al., 2015; Vinasco et al., 2006).

Different models have been proposed for the formation of these units: (i) a Permian – Triassic collisional orogen (Tahamí Terrane; Restrepo & Toussaint, 1989; Martens et al., 2014) that formed during the development of Pangea (Vinasco et al., 2006), (ii) a continental arc followed by anatexis during the Triassic (Spikings et al., 2015), (iii) a post–collisional anatectic event that formed granites at 280 Ma (Piraquive, 2017) and 228 Ma (Vinasco et al., 2006), and (iv) a continental arc that was along the western boundary of the Neoproterozoic basement (Cardona et al., 2010b; Rodríguez et al., 2014, 2017).

The description of plutons that comprise the Permian arc on the western boundary of the Chibcha Terrane presented in this study was conducted by the Servicio Geológico Colombiano (SGC) and from a compilation of previous studies (Cardona et al., 2010b; Leal–Mejía, 2011; Piraquive, 2017; Restrepo et al., 2011; Rodríguez et al., 2014, 2017; Villagómez, 2010). The plutons that form the Permian arc defined in this study are along the eastern margin of the Central Cordillera and in the Upper Magdalena Valley (La Plata Granite sensu Rodríguez, 1995a; Leal–Mejía, 2011; Rodríguez et al., 1998, 2017; Velandia et al., 1999, 2001a; the Ortega Granite, this study), serranía de San Lucas (Nechí Gneiss sensu Restrepo et al., 2011; Leal–Mejía, 2011; Rodríguez et al., 2014), and Sierra Nevada de Santa Marta (mylonitic granitoids sensu Cardona et al., 2010b, subsequently named El Encanto Orthogneiss sensu Piraquive, 2017).

We describe a new unit termed the Ortega Granite and characterize and compare the different Permian plutons using petrographic, whole–rock geochemical, and zircon U–Pb laser ablation inductively coupled plasma mass spectrometry (LA–ICP–MS) geochronological data. Regional geologic maps have been improved, and the spatial distribution of the Permian arc blocks was determined.

2. Geologic Setting

The Neoproterozoic basement of the Colombian Andes consists of blocks and tectonically scattered outcrops in the Upper Magdalena Valley (UMV), Eastern Cordillera, serranía de San Lucas, Sierra Nevada de Santa Marta, and La Guajira (Figure 1). These blocks are included in the Chibcha Terrane (Restrepo & Toussaint, 1989; Restrepo et al., 2009), recently described as the Putumayo Orogen (Ibañez–Mejia et al., 2011, 2015). Paleozoic marine sedimentary sequences overlie this basement. These rocks are intruded by Carboniferous arc plutons, such as the Carmen Stock (Leal–Mejía, 2011), and by Permian arc plutons, such as La Plata Granite (Leal–Mejía, 2011; Rodríguez et al., 2017), the Nechí Gneiss (Restrepo et al., 2011; Rodríguez et al., 2014), and the mylonitic granitoids of the Sierra Nevada de Santa Marta (Cardona et al., 2010b; Piraquive, 2017). The available geochronological data of the Permian magmatism in Colombia are outlined in Table 1. Subsequent to intrusion, local continental and marine sequences were deposited during the Triassic.

Figure 1. (a) Occurrences of Permian igneous rocks in the Colombian Andes. Modified from Gómez et al. (2015a). Data source: U–Pb zircon ages from Cardona et al. (2010b), Cochrane (2013), Cochrane et al. (2014), Gómez et al. (2015b), Leal–Mejía (2011), Piraquive, (2017), Restrepo et al. (2011), Rodríguez et al. (2017), Villagómez (2010), and this study. **(b)** Proposed distribution of metamorphic basement units in the regions related to Permian magmatism.

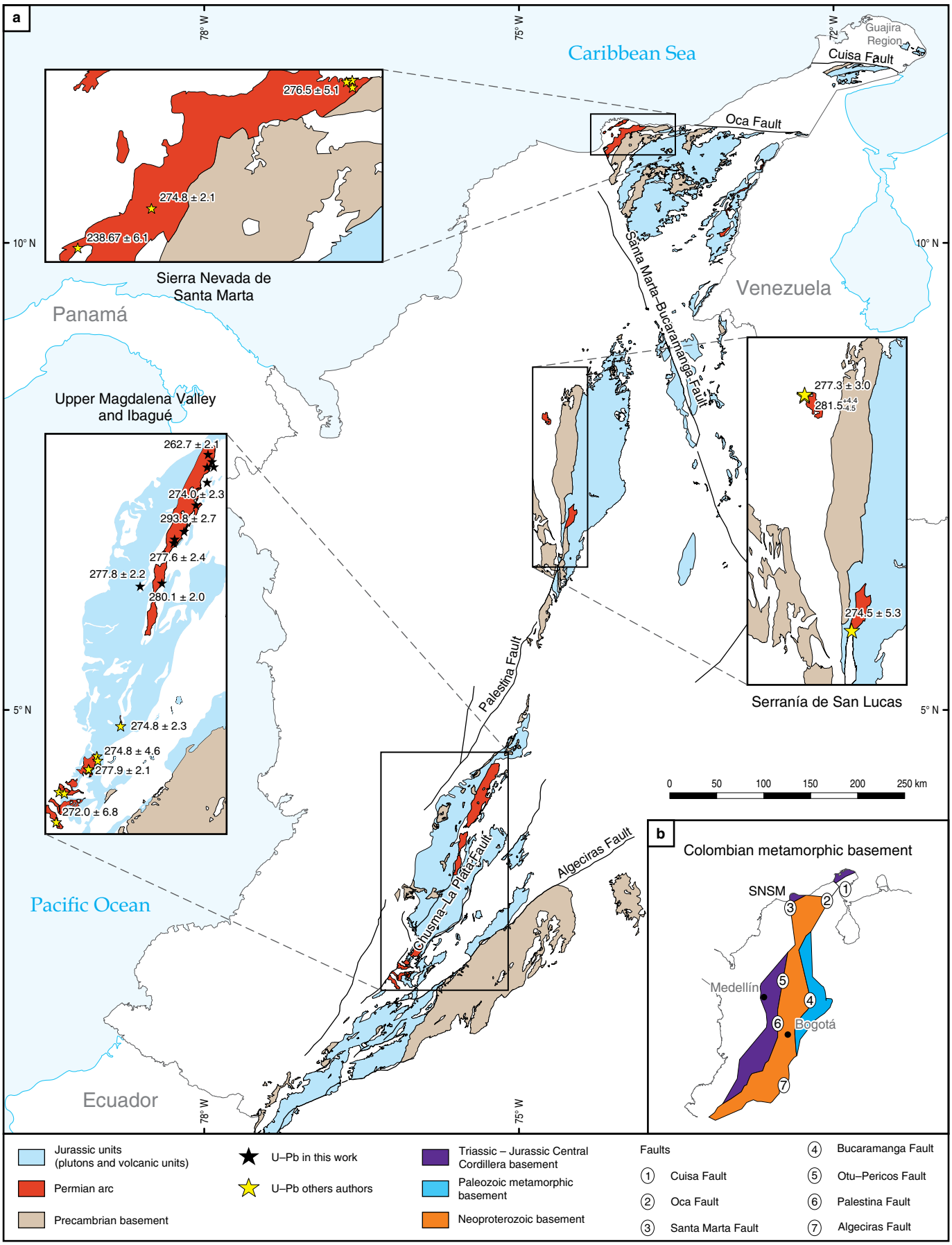
a
78° W
75° W
72° W
10° N
5° N
Caribbean Sea
Guajira Region
Cuisa Fault
Oca Fault
Santa Marta–Bucaramanga Fault
Venezuela
Panamá
276.5 ± 5.1
274.8 ± 2.1
238.67 ± 6.1
Sierra Nevada de Santa Marta
Upper Magdalena Valley and Ibagué
262.7 ± 2.1
274.0 ± 2.3
293.8 ± 2.7
277.6 ± 2.4
277.8 ± 2.2
280.1 ± 2.0
274.8 ± 2.3
274.8 ± 4.6
277.9 ± 2.1
272.0 ± 6.8
277.3 ± 3.0
281.5 +4.4 -4.5
274.5 ± 5.3
Serranía de San Lucas
Palestina Fault
Chusma–La Plata Fault
Algeciras Fault
Pacific Ocean
Ecuador
0 50 100 150 200 250 km
b
Colombian metamorphic basement
SNSM
Medellín
Bogotá
1 2 3 4 5 6 7
Jurassic units (plutons and volcanic units)
Permian arc
Precambrian basement
U–Pb in this work
U–Pb others authors
Triassic – Jurassic Central Cordillera basement
Paleozoic metamorphic basement
Neoproterozoic basement
Faults
1 Cuisa Fault
2 Oca Fault
3 Santa Marta Fault
4 Bucaramanga Fault
5 Otu–Pericos Fault
6 Palestina Fault
7 Algeciras Fault

Table 1. Previous geochronology of Permian units in Colombia.

Sample	Lithology	Latitude N	Longitude W	$^{238}U/^{206}Pb$ age (Ma) ± 2σ	MSWD	Inheritance ages (Ma)	Author
Upper Magdalena Valley							
La Plata Granite							
JGB–373	Cpx–Bt–Kfs–Pl–Qtz granofels	2° 44' 32.83"	76° 11' 47.07"	268.3 ± 2.0	1.4	1140 ± 130, n = 1; 960 ± 100, n = 1	Rodríguez et al. (2017)
GR–6655	Monzogranite	2° 30' 19.78"	76° 25' 09.78"	269.0 ± 3.0	1.09	841.43 ± 64.1, n = 1	Rodríguez et al. (2017)
MIA–516	Granite	2° 32' 16.85"	76° 25' 45.69"	270.0 ± 2.7	1.06	309.55 ± 13.7, n = 1; 297 ± 11, n = 2	Rodríguez et al. (2017)
MIA–531	Quartz monzonite	2° 29' 13.03"	76° 36' 29.77"	272.0 ± 6.8	0.34	903 ± 79, n = 3	Rodríguez et al. (2017)
GR–6631	Kfs–Pl–Qtz granofels (monzogranite)	2° 41' 36.21"	76° 16' 54.62"	273.2 ± 4.1	3.5	1781 ± 66, n = 5; 1401 ± 50, n = 2; 972, n = 2; 534 ± 34, n = 5; 393 ± 14, n = 2; 315 ± 15, n = 6	Rodríguez et al. (2017)
GR–6632	Kfs–Pl–Qtz granofels (sienogranite)	2° 41' 22.12"	76° 16' 36.09"	277.9 ± 2.1	2.5	314.9 ± 4.5, n = 2; 295.8 ± 3.7, n = 3	Rodríguez et al. (2017)
GR–6643	Monzogranite	2° 53' 30.57"	76° 00' 28.91"	274.8 ± 2.3	1.9	304 ± 6.5, n = 1; 291.3 ± 3.1, n = 4	Rodríguez et al. (2017)
WR–290	Tonalite	2° 26' 10.30"	75° 54' 48.60"	274.8 ± 4.6	0.024	ca. 750	Leal–Mejía (2011)
				Ortega Pluton			
DV82	Granite	4° 17' 15.50"	75° 13' 59.20"	271.9 ± 3.7	1.2	309 to 299	Villagómez (2010)
10RC04	Metagranite	4° 19' 24.00"	75° 12' 07.00"	277.6 ± 1.6	1.2	Not reported	Cochrane (2013)
Serranía de San Lucas							
Nechí Gneiss							
GN–1	Gneiss	8° 10' 13.00"	74° 46' 55.00"	277.3 ± 3.0	1.4		Restrepo et al. (2011)
NSE–1C	Migmatite gneiss	8° 09' 57.70"	74° 46' 43.00"	281.5 +4.4/–4.5		ca. 320	Leal–Mejía (2011)
Remedios							
12023251	Hornblende biotite diorite	6° 57' 27.50"	74° 32' 29.80"	274.5 ±5.3	0.67	ca. 1200–1000	Leal–Mejía (2011)
Puerto Nare							
WR–244	Hornblende granodiorite	6° 27' 11.90"	74° 38' 57.10"	262.9 ± 4.5	1.4	ca. 1200–1000; 600; 400	Leal–Mejía (2011)
Sierra Nevada de Santa Marta							
Northern part of the Sierra Nevada de Santa Marta							
A14	Granitoid	11° 14' 26.23"	73° 47' 50.45"	288.1 ± 4.5	0.96	1210 ± 69; 800 ± 32; 730 ± 10; 615 ± 11	Cardona et al. (2010b)
A48	Granitoid	11° 14' 14.40"	73° 48' 32.56"	276.5 ± 5.1	1.8		Cardona et al. (2010b)
EAM–12–05	Mylonite	11° 14' 24.27"	73° 48' 23.99"	264.9 ± 5.1	0.0102	Significant amount: early Paleozoic and Grenvillian ages	Cardona et al. (2010b)
				Inner Santa Marta Metamorphic Belt			
MPR–33A	El Encanto Orthogneiss	11° 04' 13.58"	74° 04' 04.89"	274.8 ± 2.1		543 ± 14; 310–302	Piraquive (2017)
GLV–11	Garnet–mica schist	11° 01' 2.13"	74° 09' 59.11"	283.67 ± 6.1 (recrystallized rim over a Carboniferous core)		1. One zircon: 2235 ± 58 2. A Neoproterozoic population at 900–1200 3. Pan–African/Brasiliano 522–655 population 4. Four crystals: 463–284.2	Piraquive (2017)
MG–063	Gaira Schists (Hbl–Bt–Pl–Ms gneiss)	11° 14' 44.15"	73° 44' 26.56"	261.46 ± 2.6		Populations at around 950, 655–850, and 270. One age of ca. 468.9 ± 7.1	Piraquive (2017)

A continental volcanic arc developed in the previously described rock assemblage during the Early to Middle Jurassic and was active for approximately 30 Ma (Rodríguez et al., 2018). This arc is represented by volcanic units (Saldaña, Noreán, La Quinta, Guatapurí, and Golero Formations sensu Tschanz et al., 1969; Rodríguez et al., 2016); batholiths (Mocoa, Páez, Altamira, Algeciras, Norosí, and Pueblo Bello Batholiths sensu Hubach & Alvarado, 1932; Arango et al., 2015; Bogotá & Aluja, 1981; Rodríguez et al., 1998, 2015; Tschanz et al., 1969; Zapata et al., 2015); and smaller intrusive bodies (Figure 1).

2.1. Upper Magdalena Valley (UMV)

The Upper Magdalena Valley corresponds to a geographical division of the Magdalena River Valley, spanning from Honda, Tolima to the Magdalena River source, south of San Agustín, Huila between the Colombian Eastern and Central Cordilleras.

The UMV is underlain by a Neoproterozoic metamorphic basement that outcrops as tectonically uplifted blocks consisting of migmatites, granofels, granulites, anatectic granites, and gneisses, in granulite to high amphibolite facies, grouped in units such as the Garzón Group, Guapotón and Mancagua Gneisses, Las Minas Migmatites, and El Recreo Granite (Ibañez–Mejia et al., 2011, 2015; Jiménez–Mejía et al., 2006; Kroonenberg & Diederix, 1992; Rodríguez, 1995a, 1995b; Rodríguez et al., 2003; Velandia et al., 1996, 2001a, 2001b). Paleozoic sedimentary rocks, such as the Granadillo Limestones, La Jagua Paleozoic Group, El Hígado Formation, Cerro Neiva Sedimentary Rocks, La Batalla Limestones and Sandstones, and El Imán Formations (Cárdenas et al., 1998; Mojica et al., 1988; Núñez et al., 1984a; Stibane & Forero, 1969; Velandia et al., 1999, 2001b; Villarroel & Mojica, 1988), discordantly overlie the Neoproterozoic crystalline basement.

Permian arc granitoids (Figure 2), including La Plata Granite (Leal–Mejía, 2011; Rodríguez, 1995a; Rodríguez et al., 1998, 2017; Velandia et al., 2001a) and the southern Rovira Granitic Stocks (Cochrane, 2013; Núñez et al., 1984a; Villagómez, 2010) (Table 1), intruded the basement and the Paleozoic sedimentary rocks.

In early studies, La Plata Granite, previously termed "La Plata Massif" (Grosse, 1931; Rodríguez, 1995a) or "La Plata Orthogranite" (Velandia et al., 1999, 2001a, 2001b), was considered to be a high–grade metamorphic unit, primarily consisting of anatectic granites, migmatitic gneisses, amphibolites, and quartz–feldspar granulites, with a predominance of granites with homophonous and nebulitic structures (Rodríguez, 1995a; Velandia et al., 2001a, 2001b). However, Rodríguez et al. (2017), based on zircon morphologies and ages, suggest that these rocks belong to the roots of an extinct continental arc.

Triassic limestones and clastic sedimentites (Luisa and Payandé Formations) were deposited atop these previous units (Cediel et al., 1980; Geyer, 1973; Mojica, 1980; Núñez et al., 1984b), and Jurassic plutons and Lower to Middle Jurassic volcanic rocks (Rodríguez et al., 2018) (Figure 2) intruded and overlie the uplifted blocks delimited by thrust and strike–slip faults.

2.2. Serranía de San Lucas (SSL)

The serranía de San Lucas is northeast of the Central Cordillera and forms a rhombic N–S–trending tectonic block delimited by the Otú Fault to the west (separating it from the metamorphic basement of the Central Cordillera), recent Magdalena River deposits to the east, the Cimitarra Fault to the south, and the Espíritu Santo Fault to the north (Figures 1, 3).

This block consists of a Neoproterozoic metamorphic basement (the San Lucas Gneiss sensu Cuadros, 2012; Cuadros et al., 2014), including quartz–feldspar gneisses with amphibolite and marble lenses (Bogotá & Aluja, 1981; Feininger et al., 1972), locally covered by Paleozoic sedimentary rocks, represented by mudstones, claystones, limestones, shales, and sandstones of La Cristalina Formation (Botero, 1940; Feininger et al., 1972). These rocks are intruded by Carboniferous (Carmen Stock sensu Leal–Mejía, 2011), Permian (Nechí Gneiss and the diorite near Remedios) (Leal–Mejía, 2011; Restrepo et al., 2011; Rodríguez et al., 2014) (Figure 3; Table 1), and Lower Jurassic (Norosí Batholith sensu Ordóñez–Carmona et al., 2009; Leal–Mejía, 2011) arc plutons.

The Nechí Gneiss was initially described as the "Quartz Feldspar and Aluminous Gneiss" (González, 2001). Subsequently, it was renamed as the Nechí Gneiss (Restrepo et al., 2011) and the Metatonalitic Gneiss of the Nechí Facies (Leal–Mejía, 2011). This unit forms a 35 km long, 10 km wide strip to the east of the Nechí county (Figure 3). The unit consists of phaneritic, isotropic rocks with an igneous aspect that are white with black spots and have a medium–grained granular texture. They range between quartz diorite, tonalite, and granodiorite (Table 2) and include banded to locally folded rocks with centimeter–scale to decimeter–scale well–defined and diffuse bands. The rocks correspond to gneisses and quartz–feldspar granofels with amphibole and biotite or their igneous equivalents, such as meta–tonalites, meta–quartz diorites, and meta–granodiorites with gneissic and granofelsic structures (Rodríguez et al., 2014) (Figure 4). Rodríguez et al. (2014) identified plagioclase, alkali feldspar, quartz, hornblende, zircon, and allanite to be igneous minerals inherited from the protolith. The quartz, plagioclase, biotite, epidote, sphene, and apatite are metamorphic minerals (Table 2) that define the gneissic structure of the rock. This unit corresponds to an igneous body affected by ductile dynamic metamorphism in low amphibolite facies with non–penetrative schistosity

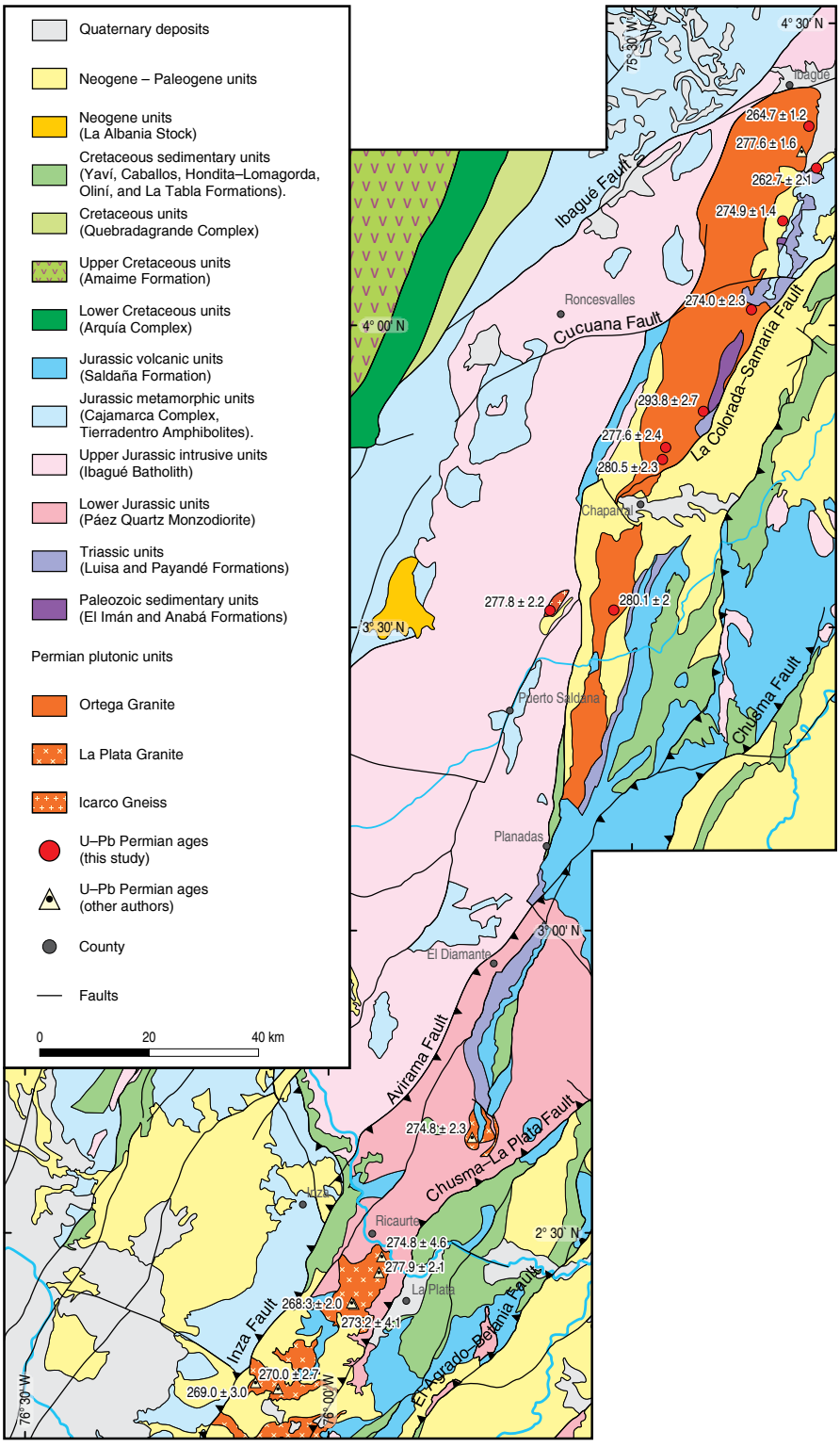

Figure 2. Geology and location of the Permian plutons in the Upper Magdalena Valley (UMV) and on the eastern slope of the Colombian Central Andes. Simplified from Gómez et al. (2015a). Data source: U–Pb zircon ages from Cochrane et al. (2014), Gómez et al. (2015b), Leal–Mejía (2011), Rodríguez et al. (2017), Villagómez (2010), and this study.

(Rodríguez et al., 2014). According to Restrepo et al. (2011), the unit has a Permian crystallization age and a Triassic metamorphic age.

The entire assemblage is covered by Lower Jurassic volcano–sedimentary successions grouped as the Noreán Formation (Clavijo, 1995; Royero, 1996), Mesozoic sedimentary and vol-

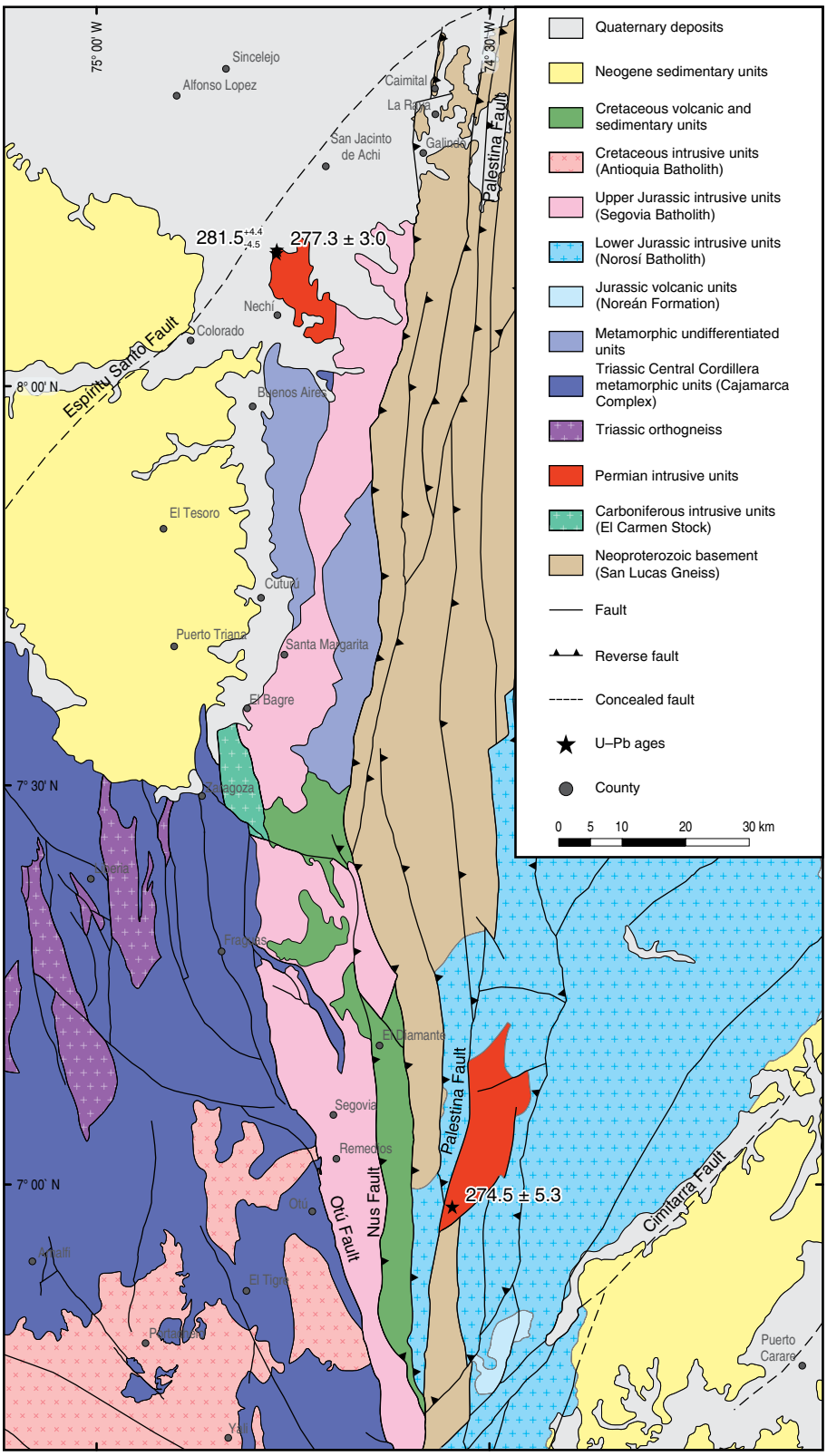

Figure 3. Geology and location of Permian plutons in the serranía de San Lucas and distribution of the U–Pb ages. Taken from Gómez et al. (2015a).

Table 2. Modal composition of rocks from the Nechí Pluton.

Sample	Latitude N	Longitude W	Qtz	Pl	Kfs	Hbl	Bt	Op	Ap	Zrn	Ttn	Ep	Petrographic classification
900563	8° 10' 12.46"	74° 46' 33.67"	26.7	34.2	0	22.6	11	0.6	Tr		2	2.9	Pl, Qtz, Hbl, Bt with Ttn gneiss
900584	8° 07' 34.19"	74° 45' 45.61"	23.8	49	13.2	4.6	6			Tr	1	2.4	Pl, Qtz, Kfs with Bt and Hbl gneiss
900585	8° 07' 50.83"	74° 46' 02.66"	17.2	36.6	4.8	13.8	14.5	Tr	Tr		3	10.1	Pl, Qtz, Bt, Hbl, and Ep gneiss
900586	8° 07' 50.83"	74° 46' 02.66"	18.8	44.4	0.7	0.7	20.8	Tr	Tr	Tr	1.4	13.2	Pl, Bt, Qtz, Ep gneiss
900588	8° 07' 35.52"	74° 45' 51.49"	39	28.1	3.1	20.1	7.9	Tr	Tr	Tr	1	0.8	Pl, Qtz, Hbl, Bt with Kfs gneiss
900589	8° 10' 01.21"	74° 46' 25.39"	12.1	56.4	0	5	7.1	0.7			4	14.7	Pl, Qtz, Hbl, Ep, Bt gneiss
900590	8° 10' 01.21"	74° 46' 25.39"	19.4	46.9	3.3	16.7	3.7	0.8			1	8.2	Pl, Qtz, Ep, Bt, Hbl with Ttn gneiss
SCC–21*	8° 07' 02.88"	74° 45' 48.27"	20	40	0	20	20					Tr	Quartz diorite
SMC–8*	8° 06' 49.43"	74° 45' 51.19"	10	20	15	30	20					4	Qtz, Pl with Bt gneiss
SMC–17*	8° 06' 55.62"	74° 45' 49.66"	25	20	10	10	25					5	Qtz, Pl with Hbl and Bt gneiss
JC011–G*	8° 07' 34.90"	74° 45' 51.46"	38	25	20		15					Tr	Qtz, Pl with Bt gneiss
JC011–X*	8° 07' 34.90"	74° 45' 51.46"	20	10		65	5				Tr	Tr	Hornblende gneiss
MI–4*	8° 08' 42.72"	74° 45' 56.28"	25	45	15		10					2	Granodiorite
JC021*	8° 07' 02.88"	74° 45' 48.27"	20	53		10	15					2	Tonalite
NPM–1*	8° 07' 26.96"	74° 45' 48.54"	10	50		40						Tr	Quartz diorite
NSE–1*	8° 09' 57.74"	74° 46' 57.72"	30		40		20					10	Migmatite granulite
NSE–2*	8° 08' 41.35"	74° 46' 01.60"	15	10	25	25	25				Tr	Tr	Quartz–feldspar gneiss

Source: Data from Rodríguez et al. (2014).
*Data from Montoya & Ordóñez–Carmona (2010).
Tr: Traces of accessory mineral.

cano–sedimentary successions and Cenozoic alluvial deposits near the edges of the block (Figure 3).

2.3. Sierra Nevada de Santa Marta (SNSM)

The Sierra Nevada de Santa Marta is a triangular block in northern Colombia, delimited by the Santa Marta–Bucaramanga Fault to the southwest, the Oca Fault to the north, and Cesar Ranchería Basin to the northeast (Figures 1, 5).

Its metamorphic basement comprises the Neoproterozoic Los Mangos Granulite and Buritaca Gneiss consisting of gneisses, anorthositic gneisses, amphibolites, anatectic granitoids, and migmatites in granulite to amphibolite facies (Ibañez–Mejia et al., 2011; Ordóñez–Carmona et al., 2002; Piraquive, 2017; Tschanz et al., 1969, 1974). These are discordantly covered by Paleozoic sedimentary units (Tschanz et al., 1969).

To the northwest, the basement is in faulted contact with the Muchachitos Gneiss and San Lorenzo Schists (Tschanz et al., 1969, 1974) of Late Jurassic age (Piraquive, 2017) (Figure 5). In addition, gabbro bodies (Tschanz et al., 1969) and Permian mylonitic granitoids, such as El Encanto Orthogneiss (Cardona et al., 2010b; Piraquive, 2017) (Table 1), are deformed and associated with the aforementioned Upper Jurassic metamorphic rocks.

The mylonitic granitoids of Valencia Creek in the Sierra Nevada de Santa Marta were described by Cardona et al. (2010b) as a body of mylonites and protomylonites that formed from quartz–feldspar rocks. Piraquive (2017) described a new unit termed El Encanto Orthogneiss (Figure 5) that includes the mylonites identified by Cardona et al. (2010b). El Encanto Orthogneiss consists of coarse–grained phaneritic rocks with amphibole bands, plagioclase, and ductilely deformed quartz veins. The unit includes mylonites and protomylonites with K–feldspar porphyroclasts (5–40 %), plagioclase (10–40 %), and biotite (<5%) surrounded by a matrix that formed during deformation and crystallization, consisting

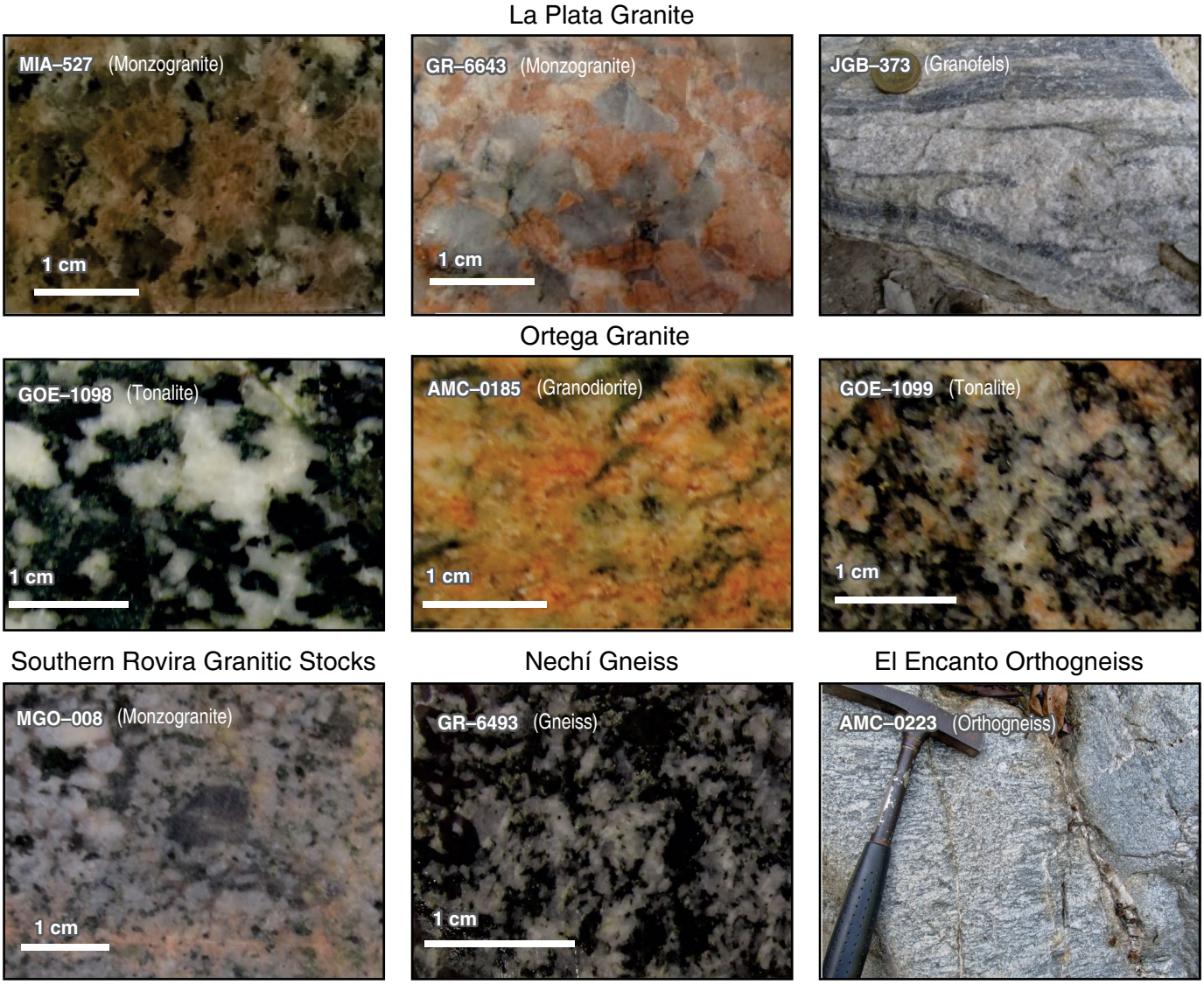

Figure 4. Macroscopic view of Permian bodies: La Plata Granite, Ortega Granite, southern Rovira Granitic Stocks, Nechí Gneiss, and El Encanto Orthogneiss.

of muscovite (5–25 %), biotite (10–30 %), quartz (20–40 %), epidote (3–20 %), chlorite, and titanite. The primary accessory minerals are zircon, titanite, apatite, and opaque minerals (Cardona et al., 2010b).

Jurassic batholiths of monzodioritic to monzogranitic composition and smaller bodies of dacitic and rhyolitic porphyries intrude the Precambrian and Paleozoic units. These are overlain by Lower to Middle Jurassic volcanic and pyroclastic rocks (Tschanz et al., 1969).

West of the Jurassic metamorphic rocks, the SNSM is formed by Upper Cretaceous to Paleogene metamorphic belts (Bustamante et al., 2009; Mora et al., 2017; Tschanz et al., 1969, 1974; Zuluaga & Stowell, 2012). Both metamorphic belts are separated by the Eocene Santa Marta Batholith (Duque–Trujillo, 2009; Tschanz et al., 1974).

2.4. Methods and Analytical Procedures

Regional cartographic studies and published articles were compiled to analyze the Permian magmatism of the UMV, SSL, and SNSM. Field control, rock sampling, petrographic, geochemical, and geochronological analyses were performed on samples collected along the eastern slope of the Central Cordillera and the UMV between Ibagué and Planadas (Figure 2). Finally, the analyses and interpretation of the results were completed including information from all tectonic blocks.

3. Petrography

All of the thin sections were analyzed using a Leitz petrographic microscope under polarized light. Mineralogical counting

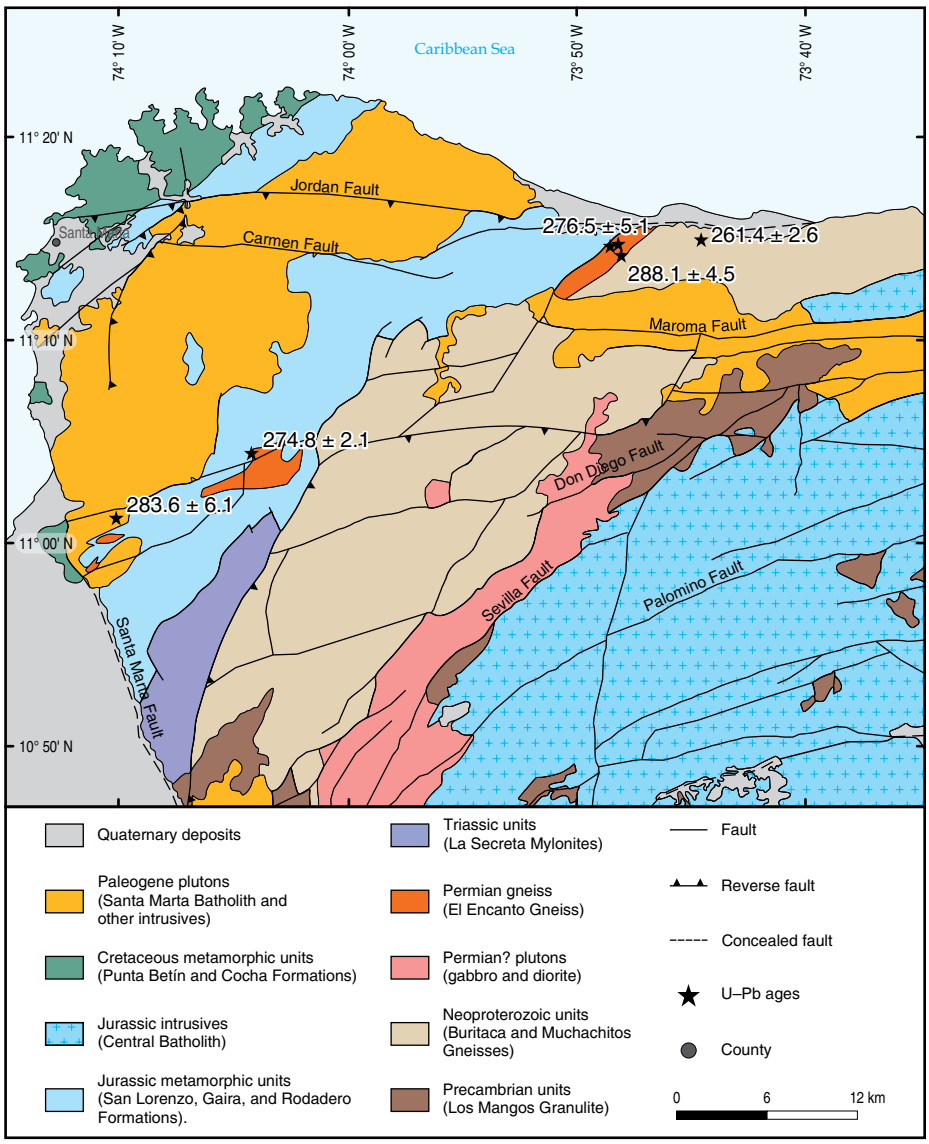

Figure 5. Geology and location of Permian plutons in the Sierra Nevada de Santa Marta and distribution of the U–Pb ages. Taken from Piraquive (2017).

was completed at 300 points per sample, identifying the primary and secondary minerals. Rocks were classified following Streckeisen (1974, 1979) considering the recommendations from Le Maitre (2002).

4. Lithogeochemistry

Whole rock geochemical analyses were performed at the laboratory of the SGC in Bogotá. Major oxides were determined using X–ray fluorescence in an analytical AXIOS Mineral spectrometer, including trace elements such as V, Mo, Nb, Ta, W, Zr, and Hf. MRC–GSR–2 and MRC–BHVO–2 were used as standards. Some elemental concentrations, such as those for Hf and Ta, were less than the detection limit of the device and are therefore not reported in the tables. Major oxides were quantified in a sample fused with lithium metaborate and tetraborate, and minor elements were quantified in a pressed sample. To interpret the major oxides, the values were recalculated considering the loss on ignition (LOI).

Trace elements were measured with inductively coupled plasma mass spectrometry (ICP–MS) using a Perkin Elmer NEXION mass spectrometer and the AGV–2 standard. The samples were gradually dissolved in strong inorganic acids (HF, HNO_3, $HClO_4$, and HCl). The process was conducted in an open system using various temperature ramps and heating times.

5. U–Pb Zircon Geochronology

U–Pb zircon dating of most samples was performed at the Laser Ablation Laboratory of the SGC. One sample (AMC–

0159A) was analyzed at the Isotopic Studies Laboratory at the Geosciences Center of the Universidad Nacional Autónoma de México (UNAM).

The concentration of zircons was obtained by panning and using a Frantz magnetic separator. Cathodoluminescence (CL) images of the crystals were acquired before isotopic analysis in the Laser Ablation Laboratory of the SGC. Some samples were photographed at the Lithological Characterization Laboratory of the Universidad Nacional de Colombia using a CITL CL8200 MK–5 adapted to a Leica DM 2500P petrographic microscope. Secondary and backscattered scanning electron microscopy – cathodoluminescence images of other samples were acquired using a JEOL scanning electron microscope, model JSM IT–300LV, equipped with secondary (SED) and backscattered (BED) electron and energy dispersive X–ray spectroscopy (EDS, OXFORD 51–XMX 1181) and cathodoluminescence (CL, Gatan miniCL EGA 0028) detectors.

Isotopic analysis was performed at the Laser Ablation Laboratory of the SGC using an inductively coupled plasma mass spectrometer ELEMENT 2™ coupled to a laser ablation system photon machines with a 193–nm excitation laser. Integration times of 0–38 s were used for the baseline, whereas integration times of 32.5–8 s were used for the samples and reference standards. The ablation points were 30 μm in diameter, and Plešovice (337.13 ± 0.37 Ma; Sláma et al., 2008), 91500 (1065 Ma; Wiedenbeck et al., 1995) and M. Dromedary (99.12 ± 0.14 Ma; Schoene et al., 2006) were used as reference standards. Data reduction was performed using the software Iolite Igor Pro, and the results were corrected for common lead according to the model of Stacey & Kramers (1975). Discordance was evaluated based on the differential between the $^{206}Pb/^{238}U$ and the $^{207}Pb/^{235}U$ ages. The sample ages were calculated using the weighted mean values of the $^{206}Pb/^{238}U$ ages for crystals <800 Ma and $^{207}Pb/^{206}Pb$ ages for crystals >800 Ma. Final results are presented discriminating to two standard deviations and plotted in Isoplot (Ludwig, 2012).

At the UNAM laboratory, zircon cathodoluminescence images were acquired using an ELM–3R luminoscope (Marshall, 1988). U–Pb isotopic analyses of zircons were performed using the laser ablation method (LA–ICP–MS) with a "Resonetics" laser, model Resolution M50, consisting of a 193 nm wavelength excimer laser LPX 220 coupled to a quadruple mass spectrometer (ICP–MS) "Thermo X–Series." The diameter of the laser beam was 23 μm. The zircon concentrations of Th, Si, P, Ti, Y, Zr, Nb, Hf, and rare earth elements (REEs) were measured during the analyses. A glass standard (NIST 610) and two natural zircon standards, a primary (91500; Wiedenbeck et al., 1995) and a secondary (Plešovice; Sláma et al., 2008), were intercalated in the analytical sequences for quality control. Methodological details are described in Solari et al. (2010).

6. Results

The Permian units described in the following phrase are geographically organized from south to north: La Plata Granite, Ortega Granite (new unit), southern Rovira Granitic Stocks (Upper Magdalena Valley and eastern slope of the Central Cordillera), Nechí Gneiss (serranía de San Lucas), and mylonitic granitoids–El Encanto Orthogneiss (Sierra Nevada de Santa Marta).

6.1. Macroscopic and Microscopic Characteristics

Forty–three igneous plutonic rocks (24 of the Ortega Granite and 19 of the southern Rovira Granitic Stocks) were studied. Table 3 presents the mineral counting of all samples analyzed. Figure 4 includes the macroscopic characteristics of the rocks present in the Permian units and Figure 6 their classification in the diagram by Streckeisen (1979).

6.1.1. Upper Magdalena Valley (UMV)

The Icarco Complex consists of amphibolites, amphibolic gneisses, feldspar–quartz gneisses, and migmatitic rocks with igneous protoliths that are considered Precambrian based on their lithological similarities to the Garzón Massif (Murillo et al., 1982). However, within this unit, Permian granitoids were identified during the present study. These occurrences were associated in the geological mapping to the Ibagué Batholith, but based on our recent findings, they are related to the Ortega Granite.

The Ortega Granite is proposed as a new unit based on its compositional and geochronological differences compared to the Upper Jurassic Ibagué Batholith (Carvajal et al., 1993; Esquivel et al., 1991; Gómez et al., 1999; Mosquera et al., 1982; Nelson, 1957; Núñez & Murillo, 1982; Núñez et al., 1984a, 1984b; Vesga & Barrero, 1978). The body is on the eastern slope of the Central Cordillera and Upper Magdalena Valley, from south of Chaparral to the Ibagué Fault to the north, between La Colorada–Samaria Fault to the east and the Avirama Fault (Figure 2) (also termed La Soledad Fault farther north) to the west.

The Ortega Granite is a heterogeneous intrusive body that consists of quartz monzodiorites, monzonites, tonalites, granodiorites, monzogranites, and rare syenogranites that are macroscopically either pink with black and white spots or white with black spots, with a predominantly granular texture and medium grain size (Figures 4, 6). It consists of quartz, plagioclase, alkali feldspar, biotite, and hornblende in addition to opaque minerals, apatite, zircon, and epidote as accessory minerals (Table 3). It locally shows microdioritic enclaves, and is intruded by andesitic, dacitic, rhyolitic, and granitic dikes; epidote veins

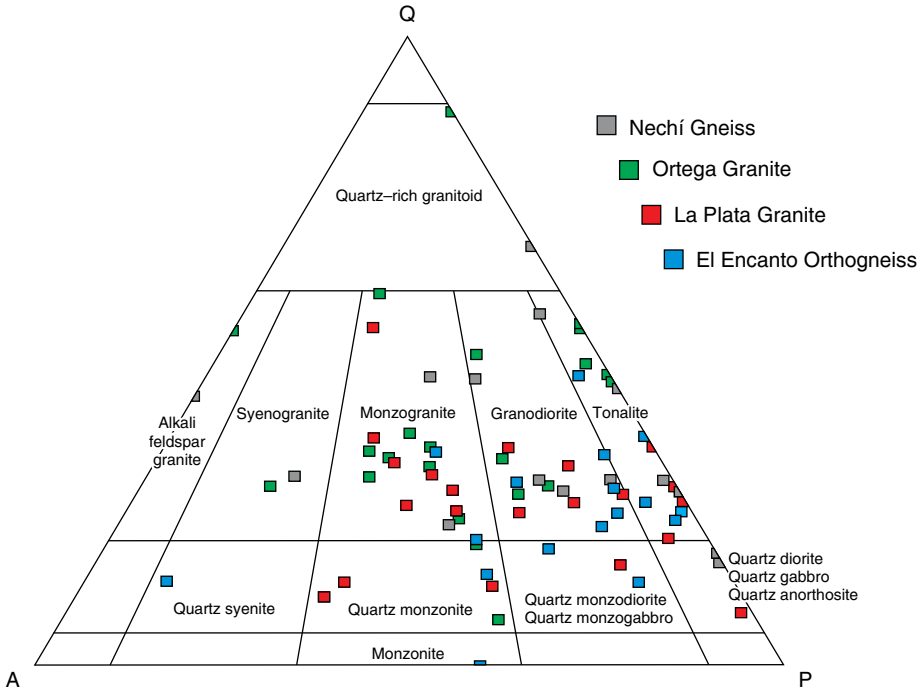

Figure 6. Modal composition of Permian granitoids in the Streckeisen triangle (1974), specified for La Plata Granite (red), Ortega Granite (green), Nechí Gneiss (gray), and El Encanto Orthogneiss (blue). Sources: Montoya & Ordóñez–Carmona (2010), Piraquive (2017), Rodríguez (1995a), Rodríguez et al. (2014, 2017).

with associated pink potassium alterations; calcite veinlets; and granitic–pegmatitic dikes.

Northeast of the Ortega Granite, Núñez et al. (1984a) defined the southern Rovira Granitic Stocks that correspond to a long intrusive body, consisting of quartz monzodiorites, quartz monzonites, monzonites, granodiorites, tonalites, and rare alkali feldspar syenites (Figure 4; Table 3). The rocks are pink or pink with black and white spots, holocrystalline, have a granular texture (Figure 4), and consist of quartz, plagioclase, alkali feldspar, biotite, and occasionally hornblende in addition to opaque, apatite, zircon, and epidote as accessory minerals (Table 3). The plutons, considered of Permian age based on their stratigraphic relations, intrude El Imán Formation (Middle Devonian) and are discordantly overlain by the Luisa (Permian – Triassic?), Payandé (Upper Triassic), and Saldaña (Lower Jurassic) Formations (Núñez et al., 1984a). These stocks are included in the Ortega Granite unit.

6.2. Geochemistry

Thirty–seven samples from La Plata Granite (red; Rodríguez et al., 2017), Ortega Granite (green), Nechí Gneiss (gray; Rodríguez et al., 2014), and mylonitic intrusions of El Encanto Orthogneiss (blue; Cardona et al., 2010b, Piraquive, 2017) were analyzed and reinterpreted (Figure 7; Table 4).

In the diagram by Middlemost (1994) (Figure 7a), the samples correspond to granites, quartz monzonites, gabbrodiorites, monzonites, and diorites similar to their petrographic classifications. The analyzed rocks have LOI values <3% that suggest low alteration, as is corroborated by the petrography, except for samples 901724 and 901725 (3.61 wt % and 4.50 wt %).

The samples from the Ortega Granite show a SiO_2 content ranging from 56.77 to 72.41 wt %, Al_2O_3 content from 14.04 to 18.80 wt %, and MgO content from 0.81 to 4.01 wt %. The Mg# ($100 \times MgO/(MgO + Fe_2O_3)$) ranges from 26.64 to 38.42. The LOI values range from 0.64 to 4.5 wt %. The SiO_2 content of the samples from La Plata Granite ranges from 58.92 to 77.39 wt %, Al_2O_3 content from 12.14 to 16.74 wt %, and MgO content from 0.10 to 3.10 wt %. The Mg# ranges from 12.20 to 31.57. The LOI values range from 0.25 to 1.06 wt % (Table 4).

In the samples from the Nechí Gneiss, the SiO_2 content ranges from 57.58 to 64.26 wt %, Al_2O_3 content from 14.98 to 16.52 wt %, and MgO content from 2.48 to 3.60 wt %. The #MgO ranges from 31.72 to 33.88. The LOI values range from 0.72 to 1.38 wt %. The samples from El Encanto Orthogneiss show a SiO_2 content ranging from 58.87 to 76.26 wt %, Al_2O_3 content from 11.83 to 17.60 wt %, and MgO content from 0.31 to 3.03 wt %. The Mg# ranges from 11.30 to 32.00 wt %. The LOI values range from 0.9 to 3.7 wt % (Table 5).

The AFM diagram (Figure 7b) shows that most samples plot within the field of the calc–alkaline series, except for sample A12, which is a granitic mylonite of El Encanto Orthogneiss. Figure 7c shows that regardless of the rock type and tectonic block location of the sample, the rocks show characteristics ranging

Table 3. Modal composition of Permian bodies in the Upper Magdalena Valley (UMV) and on the eastern slope of the Central Andes.

IGM	Sample	Latitude N	Longitude W	Qtz	Pl	Kfs	Hbl	Bt	Op	Ap	Zrn	Ttn	Ep	Others	Petrographic classification
Ortega Granite															
901723	GR–6869	4° 02' 39.12"	75° 18' 04.65"	7.2	78.7	1.3		12.2	0.6	Tr	Tr				Quartz diorite
157749	AN–1354	3° 37' 13.80"	75° 33' 22.39"	12.6	55.9	10.8	9	10.8	0.9	Tr	Tr	Tr			Quartz monzodiorite
901714	GOE–1102	3° 44' 20.31"	75° 31' 40.72"	9	28.1	47.2		5.6					9	1.1	Quartz monzonite
157773	GTJ–145	3° 39' 26.23"	75° 33' 37.51"	8.5	38	22.5	5	12	2.5	2	1	6.5	2		Quartz monzonite
20782	PM–3872	4° 03' 11.10"	75° 16' 46.65"	10.8	29.4	43.2	8.8	6.8	Tr	Tr	Tr				Quartz monzonite
901052	AMC–0157A	4° 03' 23.83"	75° 21' 16.01"	27	36	15	6	16	Tr	Tr	Tr				Granodiorite
901699	AMC–0185	3° 53' 02.51"	75° 22' 34.16"	31	55	12.5		1.5			Tr				Granodiorite
901709	GOE–1096	4° 02' 59.10"	75° 18' 08.18"	17.7	40.5	10.1		19	3.8		5.1	2.5		1.3	Granodiorite
20761	DMT–3585	4° 13' 50.59"	75° 15' 56.87"	21	46	20	3	10	Tr	Tr					Granodiorite
901712	GOE–1100	3° 32' 13.34"	75° 39' 00.41"	14.8	37.5		19.3	20.5	4.5	1			2.3		Meta–Tonalite
157753	AN–1391	3° 33' 36.61"	75° 34' 31.04"	22.9	29	24	3.43	6.87	2.67	5.72	1.14	3.05		1.14	Monzogranite
901062	GOE–1008	4° 17' 43.16"	75° 15' 49.19"	18.9	18.48	20.6	22.2	6.72	4.42	5.04	1.68				Monzogranite
901727	GR–6874	3° 32' 55.33"	75° 39' 46.92"	22.1	40.7	28.5	5.2	2.9	0.6	Tr	Tr				Monzogranite
77164	HC–840	3° 32' 24.05"	75° 37' 39.43"	25.9	19.8	26.5	14.1	6.7	2.35	2	0.33	1.34	0.67		Monzogranite
77165	HC–841	3° 32' 42.38"	75° 39' 52.25"	41.4	14.2	21.3	8.36	7.9	2.09	1.67	0.4	1.67	0.83		Monzogranite
20757	PM–3612	4° 13' 50.66"	75° 16' 57.66"	23	35	25	9	8	Tz						Monzogranite
20787	PM–3555	4° 12' 32.98"	75° 13' 52.75"		49	33		8.2	3.8	3.6	2.2	1	Tr		Monzonite
901104	MIG–083	4° 11' 56.98"	75° 19' 34.20"	17.3	82.7			Tr					Tr		Plagiogranite?
157756	DF–86	3° 31' 09.08"	75° 35' 32.66"	16.6	24.1	24.5	4.1	18.3	2.5	6.25	1.6				Syenogranite
901710	GOE–1098	3° 48' 40.05"	75° 26' 28.00"	14.3	40.3		13	18.2		2.6		7.8	3.9		Tonalite
901711	GOE–1099	3° 33' 27.23"	75° 30' 52.48"	20.5	47.7			20.5	4.5	1.1	5.7				Tonalite
901724	GR–6871	3° 47' 13.25"	75° 27'26.51"	23.5	56.6	6.7	0.6	12.6	Tr	Tr	Tr				Tonalite
901725	GR–6872A	3° 50' 03.73"	75° 26' 05.77"	15	55.6	3.9	7.2	17	0.7	Tr	Tr	0.6			Tonalite
20753	PM–3546	4° 12' 28.26"	75° 17' 32.71"	31	59			10	Tr				Tr		Tonalite
Southern Rovira Granitic Stocks															
20736	AC–549	4° 06' 29.29"	75°15'15.69"	25	43	18		11	Tr	Tr	Tr	4			Granodiorite
23553	Pm–4398	4° 07' 30.63"	75° 15' 25.35"	10.1	57.8	9.8	13.8	3.7	0.9	Tr	Tr	Tr		3.7	Quartz monzodiorite
23552	Pm–4374	4° 08' 05.83"	75° 14' 55.74"	16.5	53.5	19.7	7.1	1.6	0.8	Tr	Tr	0.8			Quartz monzodiorite
23544	AC–1041–A	4° 06' 44.48"	75° 14' 39.09"	13.8	50	30		6.2	Tr		1				Quartz monzonite
23566	DBL–3020A	4° 06' 15.39"	75° 15' 59.60"	10.9	41.8	25.1		7.94		2.09			12.1		Quartz monzonite
20763	DMT–3605	4° 11' 53.90"	75° 14' 08.58"	17	43	27		9	4				Tr		Quartz monzonite
901055	AMC–0159A	4° 11' 35.20"	75° 13' 58.21"	20	53.5	4	6	15	1	0.5	Tr				Dacite
23554	PM–4423	4° 07' 41.40"	75° 15' 07.37"	21.1	47.8	6.31	3.15		6.31	1.57	0.52	2.1	1.05		Granodiorite
20781	PM–3846	4° 04' 52.02"	75° 16' 35.78"	22	60	9			4	1	1				Granodiorite
23540	AC–971	4° 07' 23.17"	75° 15' 10.26"	17	50	10	6	8							Monzodiorite
901096	MGOQ–008	4° 17' 26.69"	75° 11' 28.03"	25	27	22	13	11	2		Tr		Tr		Monzogranite
20787	PM–3555	4° 12' 32.98"	75° 13' 52.75"		49	33		8.2	3.8	3.6	2.2	1	Tr		Monzonite
20768	PM–3636	4° 10' 20.56"	75° 15' 08.25"	4.94	4.18	28.1		16	7.99	0.19	0.38		0.9		Hypersthene syenite
23557	Pm–4469	4° 06' 40.19"	75° 15' 16.20"	18	55	1		18	1.4	2	2	0.5			Tonalite
23558	PM–4476	4° 06' 48.02"	75° 15' 09.08"	14.2	45.4	1.53	20	5.5	4	2.5	1.5	2.2			Tonalite
23550	PM–4345	4° 07' 56.36"	75° 15' 13.39"	22.4	51.7			10.3	4.3	4	1.72		2.89		Tonalite
23551	Pm–4361	4° 08' 00.28"	75° 15' 06.91"	37.2	40.1	3.22	4.3	2.5	5.01	2.15	0.71		1.07		Tonalite
20772	PM–3669	4° 08' 56.63"	75° 14' 40.25"	19.1	34	4		3	4.2	Tr	Tr	2.6	17.8	14.9	Tonalite
20722	AC–469	4° 05' 36.65"	75° 16' 06.51"	30	52			17	1				Tr		Tonalite

Tr: Traces of accessory mineral.

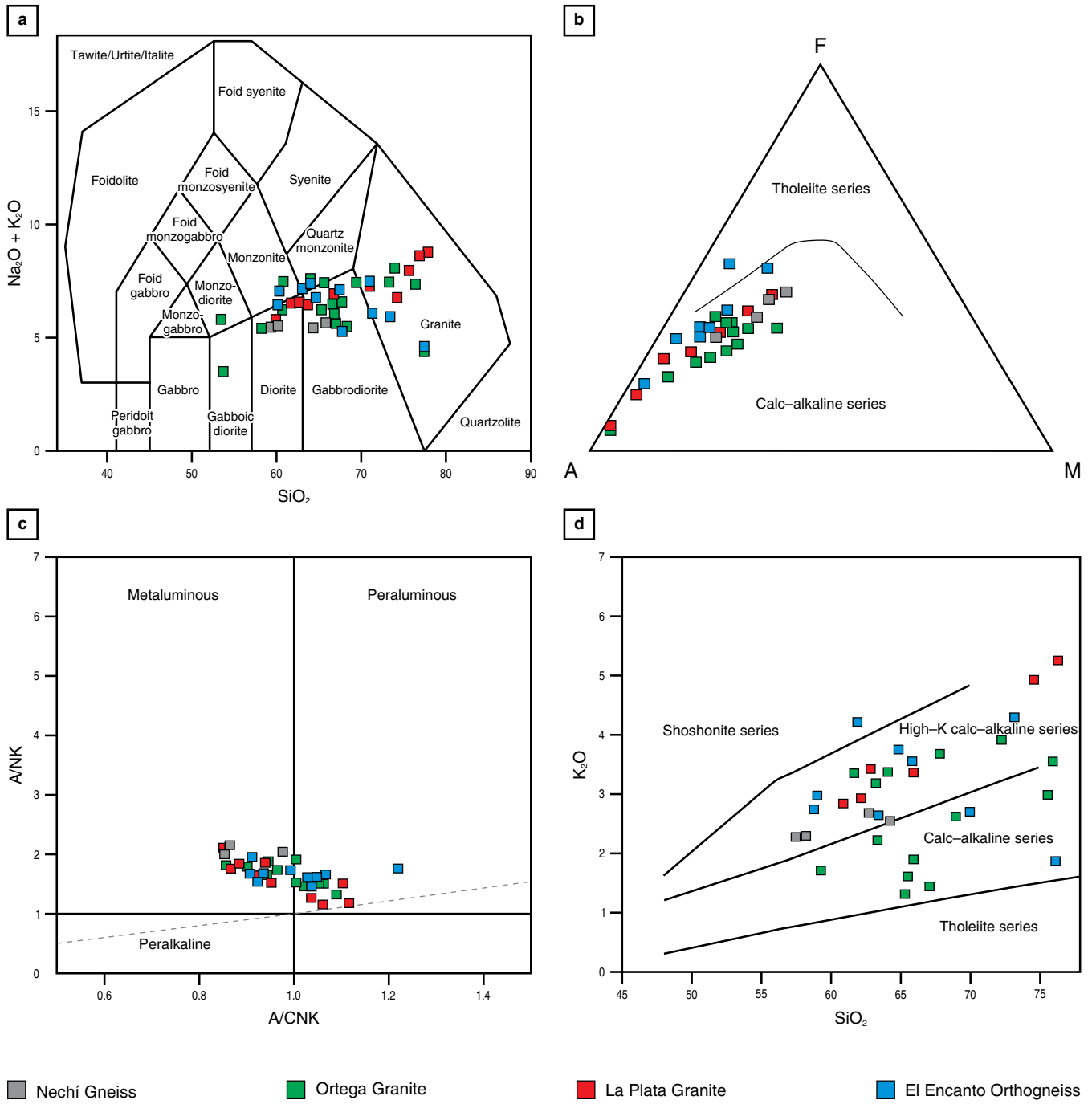

Figure 7. Classification and discrimination diagrams for Permian granitoids: **(a)** Total Alkali versus Silica (TAS) diagram by Middlemost (1994), **(b)** AFM (A (Al_2O_3 – $3K_2O$), F (FeO – TiO_2 – Fe_2O_3), and M (MgO)) diagram (Irvine & Baragar, 1971), **(c)** Alumina saturation index diagram by Shand (1943), and **(d)** Alkalinity index diagram by Peccerillo & Taylor (1976) for La Plata Granite (red), Ortega Granite (green), Nechí Gneiss (gray), and El Encanto Orthogneiss (blue). Data sources: Cardona et al. (2010b), Piraquive (2017), Rodríguez et al. (2014, 2017), and this study.

from metaluminous ($Al_2O_3 > CaO + Na_2O + K_2O$) to peraluminous ($Al_2O_3 > CaO + Na_2O + K_2O$), except for the rocks from the Nechí block that clearly show a metaluminous character.

The Peccerillo & Taylor (1976) diagram (Figure 7d) shows that the samples belong to the calc–alkaline and high–K calc–alkaline series.

The N–MORB–normalized (Sun & McDonough, 1989) samples from La Plata Granite, Ortega Granite, Nechí Gneiss, and El Encanto Orthogneiss show similar patterns of enrichment in large–ion lithophile elements (LILEs) more so than high field strength elements (HFSEs) and rare earth elements (REEs). An exception is El Encanto Orthogneiss in which

Table 4. Major and trace elements of samples from La Plata Granite (retrieved from Rodríguez et al., 2017) and Ortega Granite (this study).

Sample	900724	900729	900806	900802	900807	900732	900723	900739	900770	900800	901049	901050	901054	901055	901062	901077	901087	901096	901709	901710	901711	901712	901714	901723	901724	901725	901727
wt %	La Plata Granite										Ortega Granite																
SiO_2	77.39	76.56	74.76	62.18	66.05	62.88	73.34	58.92	69.80	60.85	72.41	63.43	67.99	61.88	67.14	69.03	63.32	64.16	60.43	56.96	64.34	60.95	65.97	58.89	61.99	56.77	67.00
Al_2O_3	12.14	13.18	13.26	16.11	15.45	16.03	13.13	16.74	14.72	16.50	14.04	15.71	14.94	16.06	15.93	15.47	15.71	16.03	18.56	18.18	17.72	16.22	14.81	18.80	15.94	15.58	14.73
Fe_2O_3	0.68	0.72	1.58	5.59	4.24	5.61	2.43	6.72	3.21	5.98	2.23	4.46	3.20	5.34	3.19	2.80	4.85	4.87	5.18	5.98	4.02	6.34	3.94	5.83	4.95	7.89	4.02
MgO	0.10	0.10	0.30	2.38	1.69	2.51	0.43	3.10	1.11	2.46	0.81	2.50	1.78	2.17	1.99	1.33	1.92	1.90	1.50	3.03	0.99	2.84	1.65	1.60	2.46	4.01	2.04
CaO	0.32	0.14	1.08	4.87	3.84	4.44	2.67	6.20	1.86	5.00	1.27	3.88	2.33	2.50	4.04	2.21	2.74	2.84	2.94	5.83	3.06	5.46	3.22	3.12	3.74	4.27	3.92
Na_2O	1.83	3.54	3.31	3.89	3.69	3.21	2.50	3.21	3.31	3.82	3.82	4.09	3.84	4.30	4.17	4.64	4.16	4.30	5.29	4.27	4.67	3.74	4.04	5.75	3.95	3.68	3.25
K_2O	7.21	5.27	4.90	2.90	3.37	3.40	4.33	2.73	4.09	2.82	3.90	2.23	3.69	3.35	1.46	2.62	3.17	3.35	2.84	2.10	3.24	1.73	3.21	2.13	2.22	1.64	3.54
TiO_2	0.11	0.15	0.20	0.83	0.61	0.73	0.13	0.85	0.47	0.82	0.33	0.67	0.52	0.80	0.45	0.38	0.72	0.72	0.73	0.86	0.56	0.76	0.60	0.70	0.67	1.07	0.58
P_2O_5	0.02	0.02	0.05	0.34	0.21	0.20	0.06	0.26	0.16	0.34	0.08	0.16	0.15	0.31	0.14	0.11	0.28	0.28	0.27	0.28	0.18	0.21	0.17	0.27	0.18	0.33	0.14
LOI	0.25	0.44	0.44	0.57	0.58	0.73	0.80	0.90	1.00	1.06	0.98	2.62	1.41	3.02	1.37	1.15	2.81	1.24	1.84	2.25	0.82	1.45	2.22	2.53	3.61	4.50	0.64
ppm																											
Ba	253.81	217.16	748.40	1165.91	1047.58	754.58	683.79	917.29	816.96	1205.15	868.88	648.91	828.01	872.47	432.33	1579.59	1044.35	1186.88									
Cs	5.29	2.23	4.17	2.62	3.22	5.05	3.21	3.26	5.49	3.32	0.89	0.95	1.98	2.76	0.63	1.35	1.53	1.68									
Co	7.75	8.77	9.91	20.96	16.16	20.83	18.51	21.84	16.05	20.84	14.47	17.54	16.09	19.31	19.76	19.00	18.03	19.50									
Sc	0.34	2.43	3.70	16.14	12.49	16.53	4.97	20.75	9.04	17.19	8.88	19.49	13.87	14.36	11.55	9.93	13.02	13.90									
Ga	11.84	14.78	14.95	23.02	22.26	19.44	13.92	21.66	22.99	24.45																	
Nb	5.20	15.90	9.00	9.30	10.90	10.00	3.10	7.10	10.60	9.10	9.50	9.20	8.60	10.30	5.20	11.20	8.40	9.40									
Rb	190.53	181.49	217.68	93.71	142.39	136.23	142.78	106.86	166.24	106.14	133.70	75.92	146.35	114.21	29.34	74.27	82.31	104.12									
Sr	250.79	48.98	157.12	724.88	592.08	509.07	390.44	685.75	413.08	780.90	219.07	388.14	384.00	553.70	722.21	788.48	712.58	810.03									
Th	31.63	30.30	25.33	13.79	21.26	18.96	9.69	11.58	38.77	11.05																	
U	5.20	2.66	7.60	4.00	5.47	4.36	4.81	1.57	8.46	3.00	4.01	1.95	2.96	1.70	1.59	0.93	1.80	1.73									
Cr	1.18	1.58	10.45	21.84	22.67	13.30	19.84	17.19	21.87	20.86																	
Zr	< 130	< 130	115.40	155.40	173.90	162.87	244.30	177.67	142.40	190.40																	
Y	6.56	83.18	19.98	18.88	22.63	19.68	7.44	15.50	19.29	21.19	21.69	23.94	21.03	17.98	12.69	13.12	18.81	20.60									
La	29.83	36.84	34.30	35.66	44.65	30.37	8.17	25.95	41.36	36.26	30.78	25.24	30.09	31.98	18.08	23.00	32.55	34.55									
Ce	50.34	80.29	65.42	70.67	82.93	61.62	16.72	50.93	76.33	70.54	52.21	44.72	51.32	62.46	32.78	39.65	58.93	62.29									
Pr	5.05	7.86	7.08	8.57	9.91	7.57	1.97	6.22	8.98	9.04	6.17	5.94	6.55	8.55	4.17	4.75	7.86	7.84									
Nd	14.79	27.32	21.99	32.51	36.67	29.18	7.11	24.92	28.20	32.78	23.74	22.74	24.63	32.82	15.65	18.98	31.26	33.72									
Sm	1.91	4.35	4.37	6.46	6.84	5.24	1.37	4.72	6.02	7.02	4.23	4.50	4.88	5.72	2.82	3.28	5.28	5.69									
Eu	0.47	0.44	1.02	2.35	2.03	1.69	0.72	1.88	1.49	2.43	0.91	1.07	1.13	1.29	0.76	1.35	1.50	1.58									
Gd	1.99	4.06	4.23	5.88	6.25	4.91	1.30	4.36	5.40	6.36	4.03	4.40	4.62	5.08	2.70	3.10	4.93	5.21									
Tb	0.19	0.49	0.62	0.78	0.90	0.73	0.19	0.63	0.76	0.89	0.64	0.69	0.69	0.70	0.38	0.42	0.71	0.74									
Dy	0.83	2.08	3.41	3.99	4.50	3.63	1.00	2.95	3.94	4.58	3.31	3.70	3.53	3.28	1.95	2.16	3.46	3.69									
Ho	0.17	0.39	0.71	0.79	0.88	0.70	0.21	0.58	0.80	0.90	0.69	0.74	0.70	0.65	0.38	0.42	0.67	0.69									
Er	0.61	1.22	2.28	2.44	2.76	2.13	0.67	1.70	2.52	2.75	2.12	2.25	2.10	2.01	1.16	1.30	2.02	2.22									
Tm	0.09	0.17	0.34	0.33	0.39	0.29	0.10	0.22	0.36	0.37	0.31	0.32	0.29	0.27	0.16	0.18	0.28	0.29									
Yb	0.65	1.27	2.42	2.30	2.60	1.92	0.73	1.41	2.57	2.50	2.02	2.08	1.88	1.74	1.08	1.24	1.80	1.94									
Lu	0.11	0.20	0.39	0.36	0.41	0.28	0.12	0.22	0.39	0.38	0.33	0.33	0.29	0.27	0.17	0.20	0.28	0.30									
(La/Yb)n	30.59	19.34	9.45	10.34	11.45	10.55	7.46	12.27	10.73	9.67	10.18	8.09	10.70	12.22	11.14	12.41	12.04	11.84									
(Eu/Yb)n	2.07	0.99	1.20	2.92	2.23	2.51	2.82	3.81	1.66	2.78	1.28	1.47	1.72	2.12	2.00	3.11	2.37	2.33									
Nb/La	0.36	0.53	0.93	0.50	0.61	0.34	1.30	0.42	0.64	0.47	0.31	0.36	0.29	0.32	0.29	0.49	0.26	0.27									
#MgO	12.82	12.20	15.96	29.86	28.50	30.91	15.03	31.57	25.69	29.15	26.64	35.92	35.74	28.89	38.42	32.20	28.36	28.06									

LOI: loss on ignition; n—normalized to chondrite values of Nakamura (1974).

Table 5. Major and trace elements of samples from the Nechí Gneiss (retrieved from Rodríguez et al., 2017) and El Encanto Orthogneiss (retrieved from Cardona et al., 2010b).

Sample	900584	900588	900586	900585	A44	A13	A15	A12	A11	A21	A16	A26	24
wt %	Nechí Gneiss				Sierra Nevada de Santa Marta–El Encanto Orthogneiss								
SiO_2	64.26	58.23	62.75	57.58	70.01	76.26	65.82	58.87	59.05	63.38	61.85	65.87	65.05
Al_2O_3	14.98	15.83	15.47	16.52	16.16	11.83	15.91	17.60	16.84	16.71	16.09	15.83	14.68
Fe_2O_3	4.84	7.09	5.92	7.04	1.87	2.90	4.09	7.69	6.44	4.13	5.60	4.21	7.25
MgO	2.48	3.58	2.75	3.60	0.31	0.95	1.16	0.98	3.03	1.35	1.73	1.06	2.09
CaO	4.56	5.72	4.44	6.15	2.52	1.58	3.71	5.48	4.27	4.41	3.68	2.88	1.14
Na_2O	3.27	3.35	2.91	3.27	4.87	2.90	4.09	3.80	4.19	4.48	2.94	3.64	1.41
K_2O	2.54	2.29	2.67	2.28	2.73	1.88	3.37	2.77	3.00	2.65	4.22	3.58	3.76
TiO_2	0.59	0.85	0.69	0.83	0.19	0.39	0.54	0.79	0.88	0.55	1.11	0.52	0.73
P_2O_5	0.15	0.25	0.20	0.24	0.06	0.05	0.19	0.32	0.29	0.23	0.66	0.19	0.18
LOI	0.72	0.83	1.00	1.38	0.90	0.90	1.00	1.50	1.60	1.70	1.70	1.80	3.70
ppm													
Ba	1300.00	1130.00	769.00	996.00	1052.70	1029.00	1052.30	790.60	746.10	841.40	1321.90	1205.40	639.20
Cs	1.30	6.60	5.50	2.30	0.40	2.40	1.70	2.70	2.20	2.50	1.60	1.50	2.20
Co	21.00	27.00	25.00	29.00	1.30	5.80	6.90	6.50	14.60	5.90	9.10	6.40	12.90
Sc	16.00	20.00	16.00	21.00	2.00	6.00	6.00	8.00	16.00	6.00	9.00	6.00	14.00
Ga	17.00	20.00	19.00	20.00									
Nb	6.50	8.60	5.40	8.50	7.70	8.30	25.20	20.10	15.70	24.00	18.30	23.90	16.00
Rb	62.00	84.00	118.00	84.00	43.00	67.60	90.80	92.50	107.70	97.40	128.40	105.30	109.20
Sr	516.00	668.00	524.00	676.00	674.10	285.80	694.10	763.50	560.00	757.90	362.10	575.70	123.90
Th	11.00	8.00	11.00	7.90									
U	1.60	5.20	1.00	1.60	1.70	1.90	5.90	5.50	3.50	3.80	1.00	4.30	4.00
Cr	40.00	54.00	49.00	49.00									
Zr	178.00	163.00	148.00	141.00	82.70	197.80	199.40	219.60	176.00	200.00	281.70	178.60	183.60
Y	19.00	20.00	12.00	19.00	9.20	9.10	23.10	29.10	30.90	24.00	24.60	22.70	33.20
La	48.00	35.00	42.00	33.00	7.80	33.70	36.10	30.60	30.40	38.80	59.60	28.30	35.10
Ce	92.00	73.00	85.00	69.00	16.60	73.20	74.30	70.50	79.80	78.40	149.00	64.00	78.30
Pr	8.40	7.40	7.90	7.10	1.98	8.13	7.85	8.48	10.18	8.48	19.46	7.29	9.16
Nd	25.00	27.00	24.00	25.00	8.40	28.60	27.90	33.30	40.40	31.40	80.60	27.70	34.60
Sm	5.80	6.00	4.80	5.60	1.63	4.62	5.10	6.69	7.42	5.81	14.13	5.08	6.62
Eu	1.90	1.90	1.30	1.80	0.59	0.98	1.37	1.85	1.54	1.48	2.04	1.25	1.46
Gd	5.20	5.40	4.40	5.10	1.47	2.93	3.91	5.17	5.75	4.51	9.82	4.31	5.73
Tb	0.71	0.75	0.51	0.73	0.27	0.45	0.66	0.89	0.95	0.76	1.22	0.72	1.07
Dy	3.80	4.00	2.50	3.90	1.33	1.78	3.31	4.37	5.05	3.83	5.17	3.74	5.13
Ho	0.73	0.80	0.48	0.76	0.25	0.31	0.65	0.87	0.94	0.73	0.77	0.70	0.97
Er	2.30	2.50	1.40	2.30	0.78	0.75	2.04	2.63	2.72	2.30	2.02	2.16	2.95
Tm	0.30	0.31	0.17	0.31	0.14	0.12	0.33	0.39	0.43	0.32	0.22	0.32	0.41
Yb	2.00	2.10	1.10	2.10	0.96	0.76	2.21	2.81	2.63	2.28	1.32	2.15	2.94
Lu	0.30	0.32	0.18	0.31	0.16	0.14	0.35	0.44	0.36	0.35	0.18	0.35	0.43
(La/Yb)n	16.00	11.11	25.45	10.48	5.42	29.56	10.89	7.26	7.71	11.35	30.10	8.78	7.96
(Eu/Yb)n	2.71	2.59	3.38	2.45	1.76	3.68	1.77	1.88	1.67	1.85	4.42	1.66	1.42
Nb/La	0.33	0.33	0.50	0.41	0.00	0.00	0.00	0.00	0.00	0.00	0.00	0.00	0.00
#MgO	33.88	33.55	31.72	33.83	14.22	24.68	22.10	11.30	32.00	24.64	23.60	20.11	22.38

LOI: loss on ignition

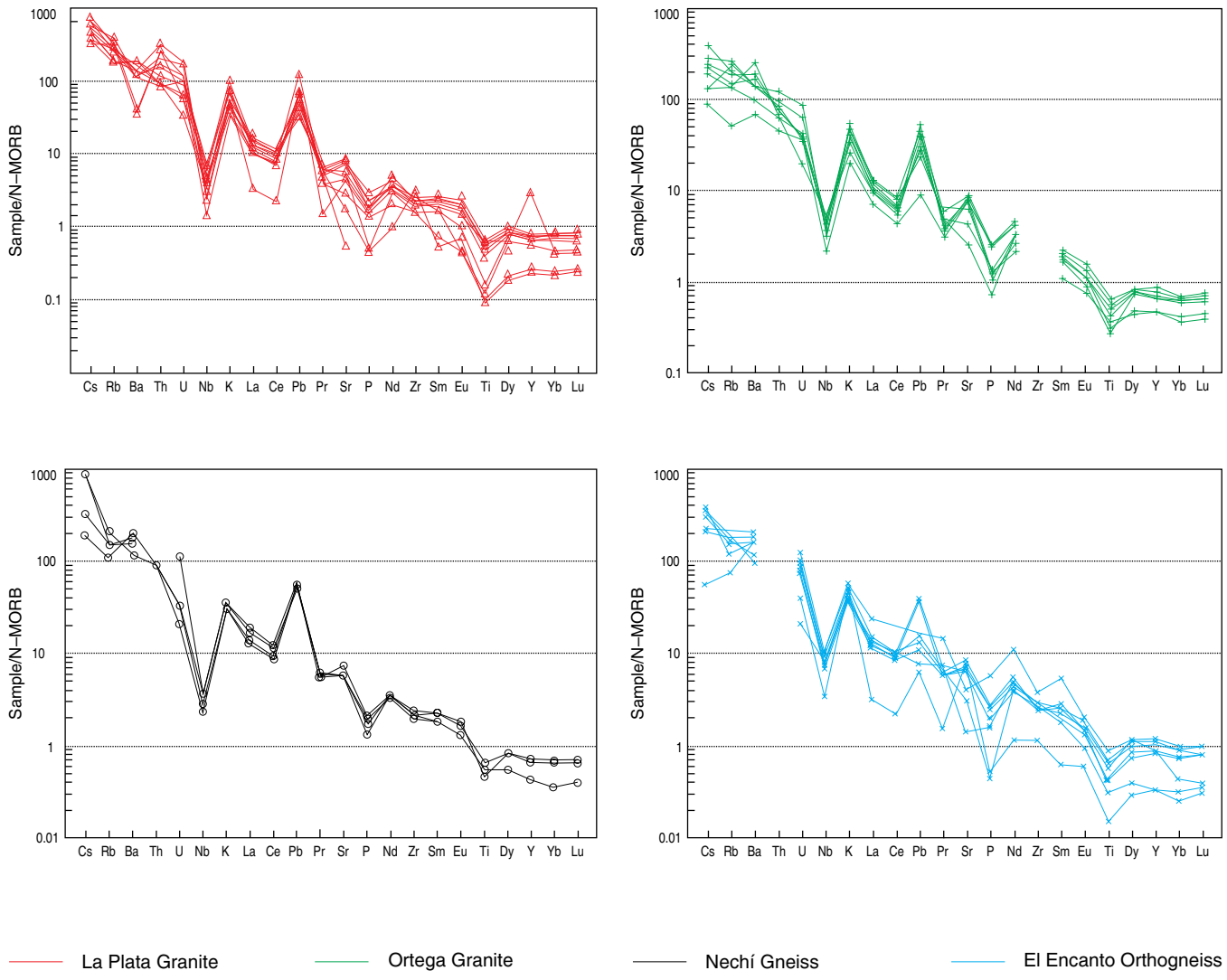

Figure 8. Normal Mid–Ocean Ridge Basalt (N–MORB) normalized trace element diagrams (Sun & McDonough, 1989) for La Plata Granite (red), Ortega Granite (green), Nechí Gneiss (black), and El Encanto Orthogneiss (blue). Data sources: Cardona et al. (2010b), Piraquive (2017), Rodríguez et al. (2014, 2017), and this study.

some samples present more dispersed patterns (Cardona et al., 2010b). The bodies show negative Nb, P, and Ti anomalies and enrichment in Cs, Ba, and K (Figure 8) that are typical of a continental arc environment formed in a subduction tectonic regime.

Chondrite–normalized (Nakamura, 1974) REEs show enrichment in light over heavy rare earth elements with a negative slope (Figure 9). These patterns are similar to those of rocks generated above subducting plates.

The Ortega Granite shows values of (La/Yb)n = 8.09–12.41, and La Plata Granite values range from 7.46 to 12.27 with two high values (19.34–30.59) corresponding to samples 900724 and 900729. The samples from the Nechí Gneiss show (La/Yb)n values ranging from 10.48 to 25.45. El Encanto Orthogneiss shows (La/Yb)n ratios = 5.42–11.35, and samples A13 and A16 have high (La/Yb)n values ranging from 19.2 to 30 (related to SiO_2 values higher than 75 wt %).

The Eu/Eu* anomaly is negative in most cases, with values ranging from 0.69 to 0.95, suggesting Eu fractionation by plagioclase crystallization. Most samples from the Ortega Granite show negative Eu anomalies, with values of Eu/Eu* = 0.68–0.89, and one sample has a value of Eu/Eu* = 1.30. The samples from La Plata Granite show negative (Eu/Eu* = 0.32–0.95) and positive (Eu/Eu* = 1.02–1.117) Eu anomalies (samples 900732, 900800, 900802, 900739) that could indicate plagioclase accumulation. The Nechí Gneiss shows positive Eu anomalies with values of Eu/Eu* = 1.03–1.06 except for sample 900586 (Eu/Eu* = 0.87). El Encanto Orthogneiss shows values

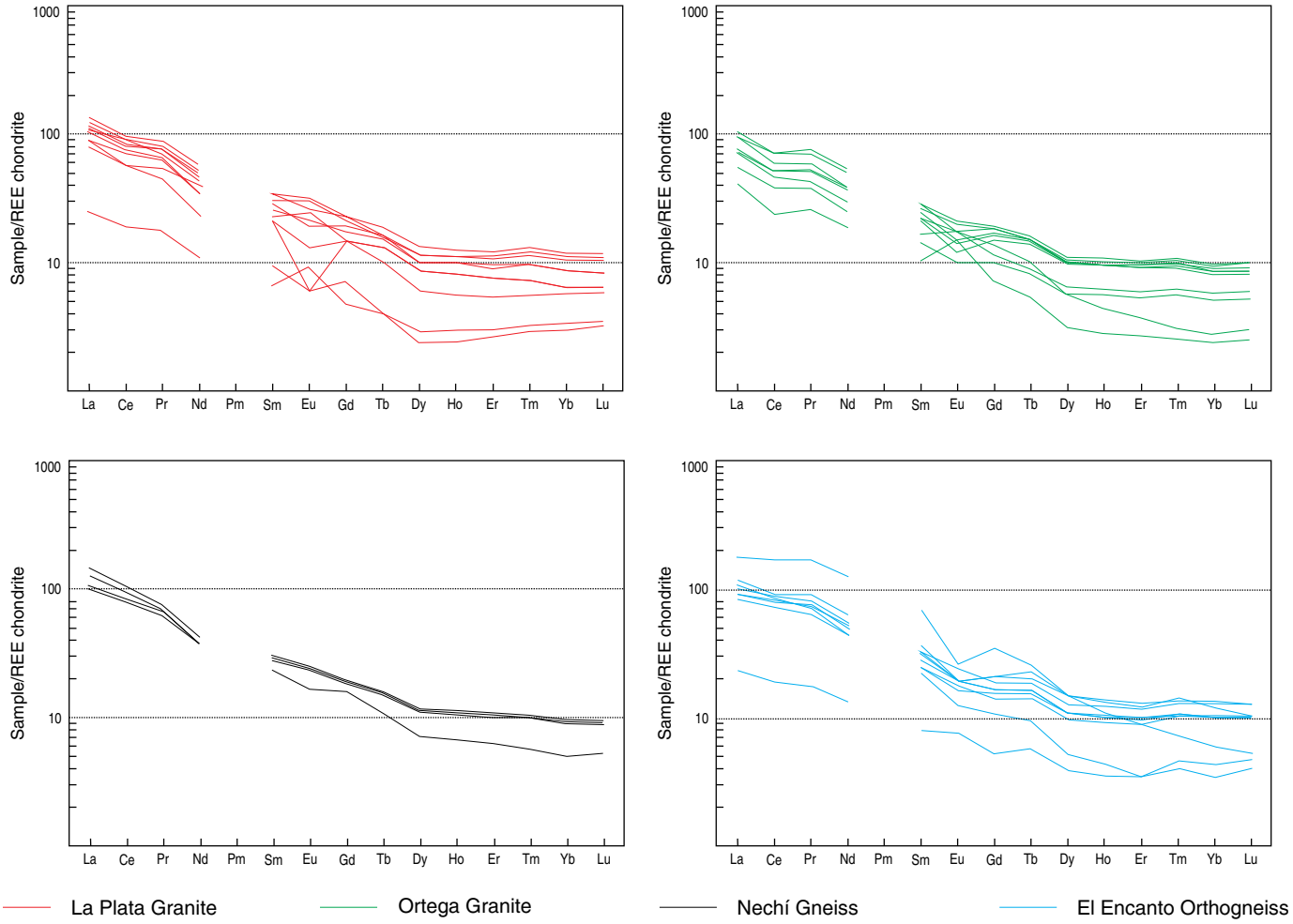

Figure 9. Chondrite–normalized rare earth element (REE) diagrams (normalizing values after Nakamura, 1974) for La Plata Granite (red), Ortega Granite (green), Nechí Gneiss (black), and El Encanto Orthogneiss (blue). Data sources: Cardona et al. (2010b), Piraquive (2017), Rodríguez et al. (2014, 2017), and this study.

of Eu/Eu* = 0.72–0.94 and a positive Eu anomaly of Eu/Eu* = 1.17 (sample A44).

The analyzed granitoids have high ratios of (La/Yb)n versus Sr/Y that place them within the continental arcs (Figure 10a) because of the garnet retention of heavy rare earth elements and Y, reflecting deep melting in a convergent margin (Condie & Kröner, 2013). In the Chappell & White (1974) discrimination diagram, most samples fall within the type–I granite field (Figure 10b).

6.3. Geochronology

A total of nine samples were dated in this study using the U–Pb zircon LA–ICP–MS method: one sample (GOE–1100) from the Icarco Complex, six samples (GOE–1099, GOE–1098, GR–6872B, AMC–0185, GOE–1096, and JPZ–010A) from the Ortega Granite, and two samples (AMC–0159A and MGOQ–008) from the southern Rovira Granitic Stocks. The locations of the samples are shown in Figure 2, and the resulting ages are outlined in Table 6. The nomenclature used for the inherited zircons followed the definitions of Miller et al. (2007) and Siégel et al. (2018).

The zircons of sample GOE–1100 are prismatic subhedral to short prismatic, ranging in size from 50 × 90 μm to 100 × 200 μm. Under CL, two different textures showed: low–luminescence homogeneous zones with intermediate–luminescent edges, and zones with different and irregular luminescence (Figure 11). Crystals with concentric zoning patterns are scarce. Any analysis with a discordance higher than 10% was disregarded during interpretation. Four inherited ages were obtained (Table 6): two that were Neoproterozoic, one Late Ordovician, and one Late Pennsylvanian. The principal group of ages ranges from 298 to 260 Ma, and the weighted mean average of the concordant data is 277.8 ± 2.2 (MSWD = 2.4) (Figure 12), which is interpreted as the age of the igneous crystallization. Forty–nine crystals show a Th/U ratio higher than 0.31, with a mode of 0.79, which is associated with the values of igneous zircons

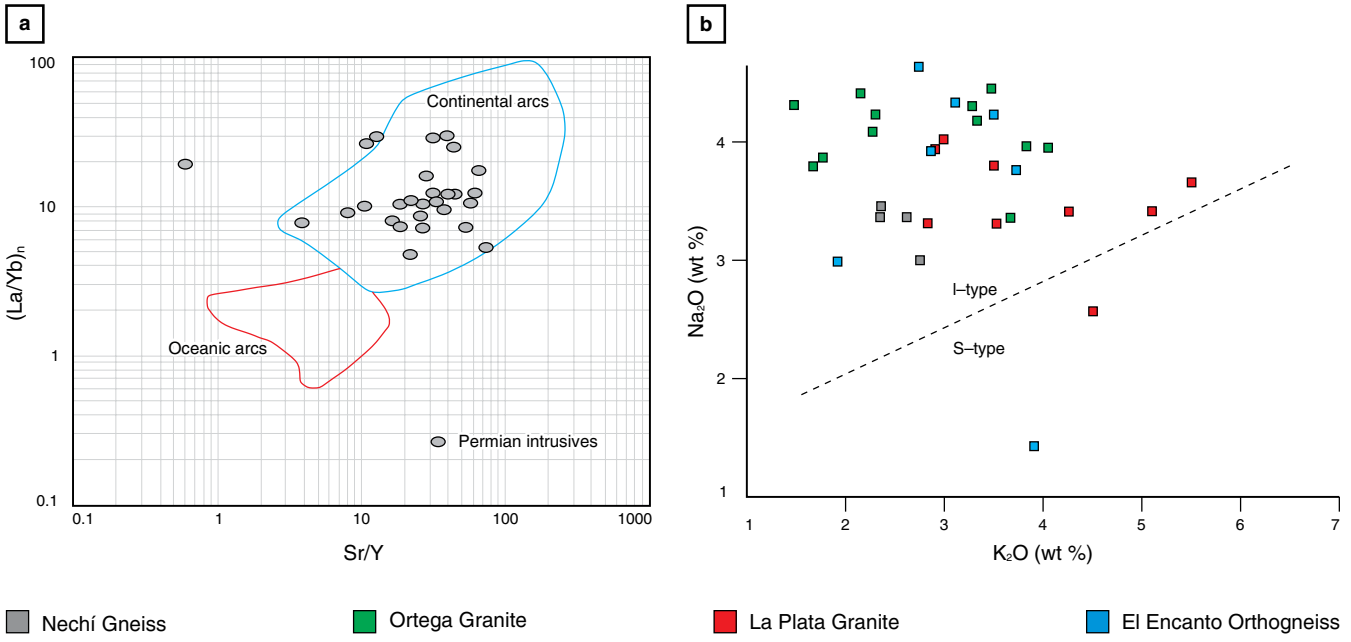

Figure 10. Tectonic environment discrimination diagrams for Permian units. **(a)** Condie & Kröner (2013) diagram. **(b)** Chappell & White (1974) diagram.

Table 6. Geochronological results of this study.

Sample	Lithology	Latitude N	Longitude W	$^{238}U/^{206}Pb$ age (Ma) ± 2σ	MSWD	Inheritance ages (Ma)
Upper Magdalena Valley						
Icarco Complex						
GOE–1100	Metatonalite	3° 32' 13.34"	75° 39' 00.41"	277.8 ± 2.2	2.4	990 ± 46; 911 ± 32; 457 ± 16; 304 ± 11
Ortega Granite						
GOE–1099	Tonalite	3° 33' 27.23"	75° 30' 52.48"	280.1 ± 2.0	1.9	300.1 ± 7.5 – 292.1 ± 9.3, n = 5
GOE–1098	Tonalite	3° 48' 40.05"	75° 26' 28.00"	280.5 ± 2.3	2.2	322.8 ± 8.0; 319.8 ± 8.0; 322.8 ± 8.0; ca. 305 ± 8.0, n = 2; ca. 304 ± 8.0, n = 2; 299.4 ± 8.7
GR–6872B	Dyke of tonalite	3° 50' 03.73"	75° 26' 05.77"	277.6 ± 2.4	2.2	304.3 ± 11.8
AMC–0185	Granodiorite	3° 53' 02.51"	75° 22' 34.16"	293.8 ± 2.7	2.1	363 ± 16 – 362 ± 14, n = 2; 332.7 ± 9.3 – 309.7 ± 9.9, n = 22
GOE–1096		4° 02' 59.10"	75° 18' 08.18"	274.0 ± 2.3	1.04	954 ± 39; 326 ± 11.8; 312 ± 7.5; 311 ± 5.9; 306 ± 11 – 287 ± 8, n = 34; 285 ± 9 – 279 ± 9, n = 15
JPZ–010A	Granodiorite	4° 22' 09.12"	75° 13' 39.12"	264.7 ± 1.2	1.8	312 ± 8; 307.7 ± 7.5; 286–281 (mean = 282.9 ± 2.8; n = 7)
Southern Rovira Granitic Stocks						
AMC–0159A	Dacite	4° 11' 35.20"	75° 13' 58.21"	274.9 ± 1.4	0.96	
MGOQ–008	Monzogranite	4° 17' 26.69"	75° 11' 28.03"	262.7 ± 2.1	1.6	1104 ± 80; 924 ± 54; 345 ± 11; 307.8 ± 9.3; 281 ± 7 – 275 ± 4, n = 4

Data for GOE–1100, GOE–1099, GOE–1098, GR–6872B, AMC–0185, GOE–1096, JPZ–010A, AMC–0159A, and MGOQ–008 is included in the Tables 1–7 of the Supplementary Information.

n: number of results in the ages range.

(Rubatto, 2002). Notably, the zircon textural characteristics observed under CL and the wide age range suggest a process of zircon recrystallization or modification after initial crystallization; however, the time limit between both processes could not be defined based on available data. Three concordant younger age results (ca. 245 Ma, ca. 242 Ma, and ca. 223 Ma with a Th/U of 0.76, 0.14, and 0.22, respectively) were excluded from the calculation of the mean age.

In sample GOE–1099, the zircons are prismatic, euhedral, some having bipyramidal terminations, and reaching up to 150 μm

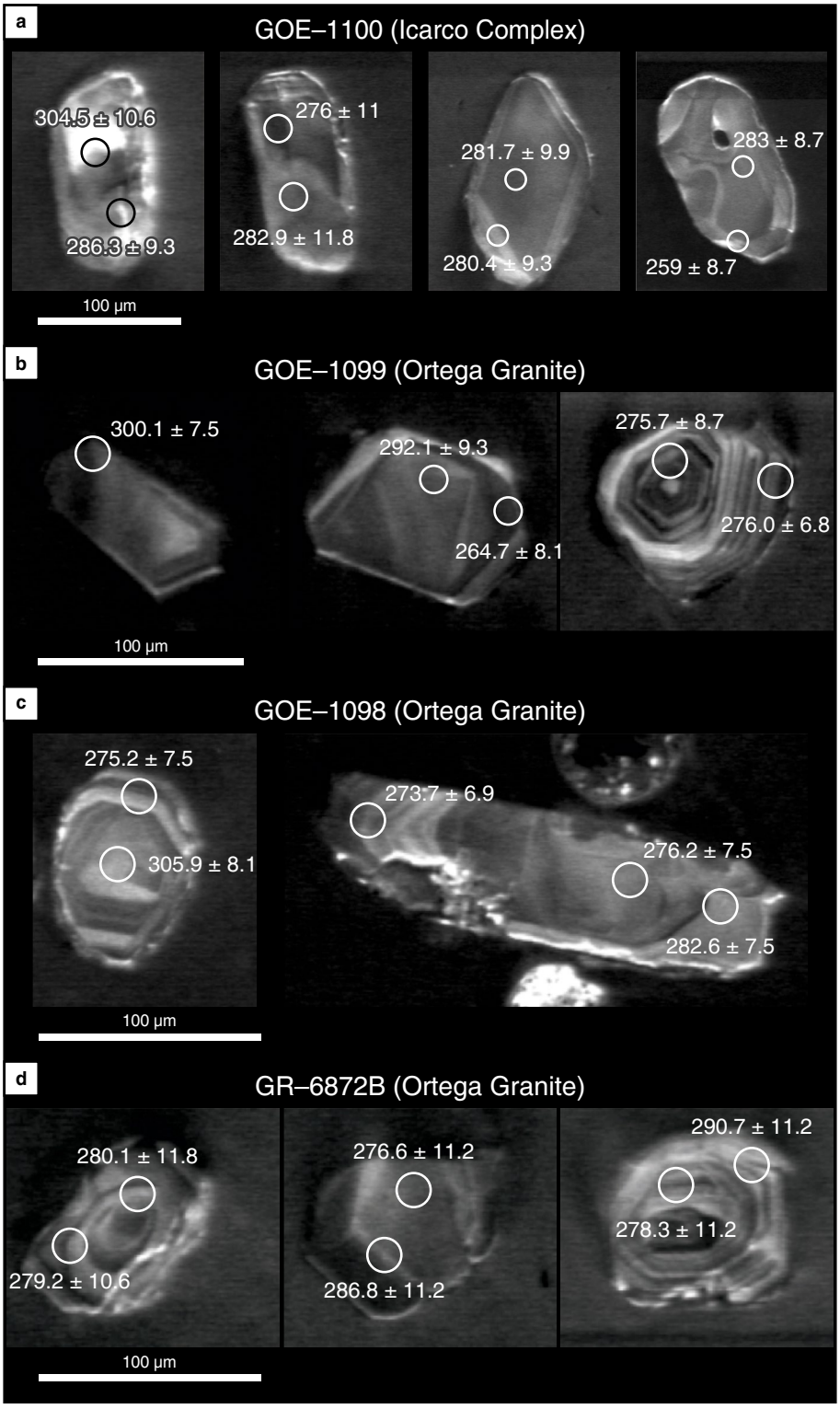

Figure 11. Cathodoluminescence images of representative zircons from samples: **(a)** GOE–1100, **(b)** GOE–1099, **(c)** GOE–1098, and **(d)** GR–6872B.

along their largest dimension. Under CL, nearly all crystals show concentric zoning patterns and have a few inherited cores (Figure 11). Four analyses showed discordances higher than 10%, and these were discarded during interpretation. Textural and temporal differences are observed between the zircon cores

Figure 12. Tera–Wasserburg concordia diagrams and medians and/or means of Permian samples of plutons from the Icarco Complex and the Ortega Granite. Gray ellipses: discarded results; blue ellipses: analysis of inherited zircons and anticrystals; green ellipses: Permian igneous ages; light yellow ellipses: Triassic results with no known geological meaning thus far.

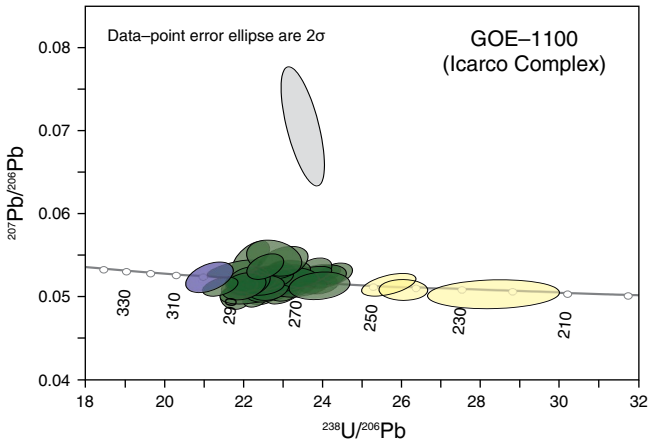
Data–point error ellipse are 2σ
GOE–1100
(Icarco Complex)
$^{207}Pb/^{206}Pb$
$^{238}U/^{206}Pb$

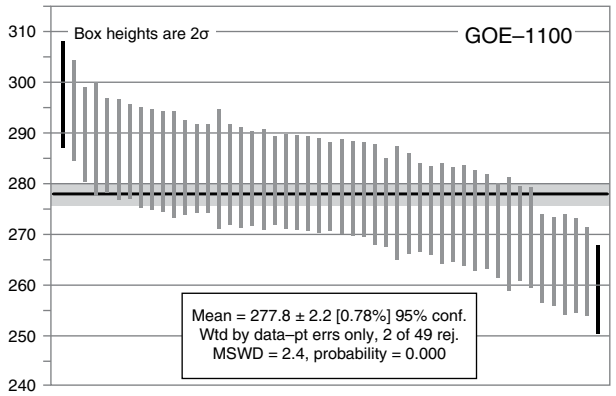
Box heights are 2σ
GOE–1100
Mean = 277.8 ± 2.2 [0.78%] 95% conf.
Wtd by data–pt errs only, 2 of 49 rej.
MSWD = 2.4, probability = 0.000

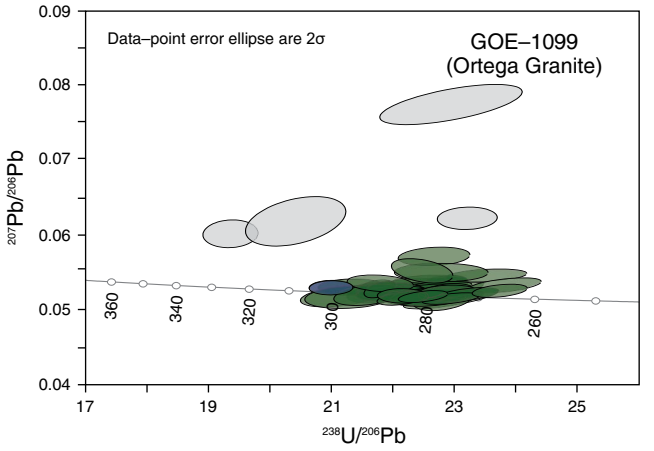
Data–point error ellipse are 2σ
GOE–1099
(Ortega Granite)
$^{207}Pb/^{206}Pb$
$^{238}U/^{206}Pb$

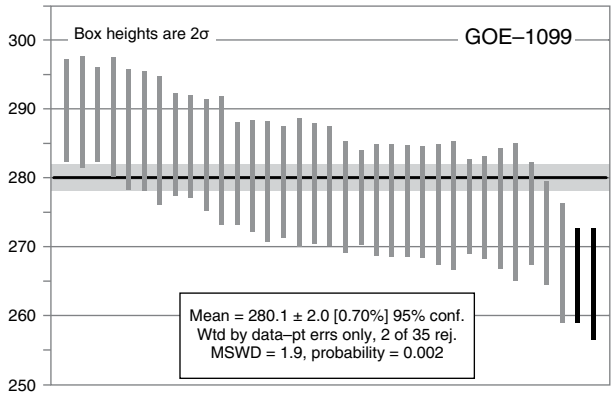
Box heights are 2σ
GOE–1099
Mean = 280.1 ± 2.0 [0.70%] 95% conf.
Wtd by data–pt errs only, 2 of 35 rej.
MSWD = 1.9, probability = 0.002

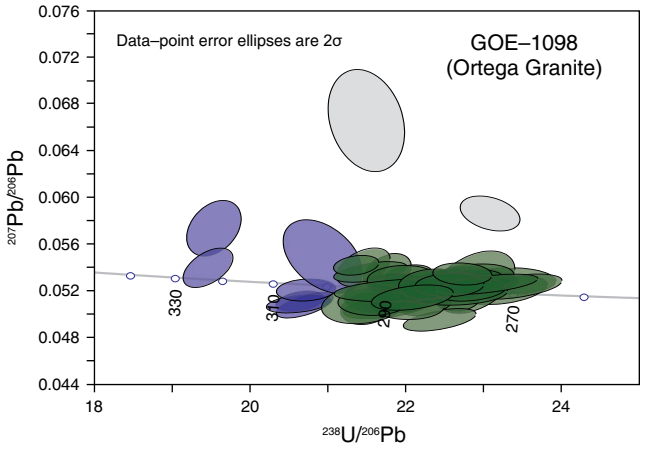
Data–point error ellipses are 2σ
GOE–1098
(Ortega Granite)
$^{207}Pb/^{206}Pb$
$^{238}U/^{206}Pb$

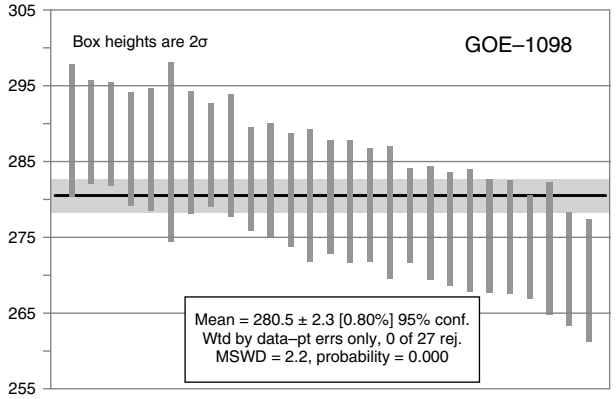
Box heights are 2σ
GOE–1098
Mean = 280.5 ± 2.3 [0.80%] 95% conf.
Wtd by data–pt errs only, 0 of 27 rej.
MSWD = 2.2, probability = 0.000

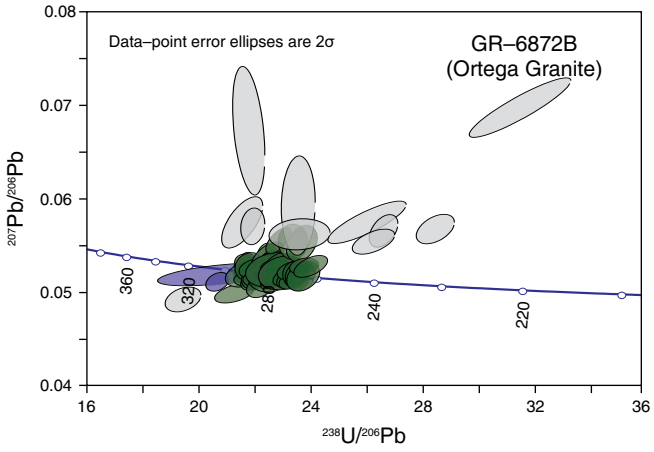
Data–point error ellipses are 2σ
GR–6872B
(Ortega Granite)
$^{207}Pb/^{206}Pb$
$^{238}U/^{206}Pb$

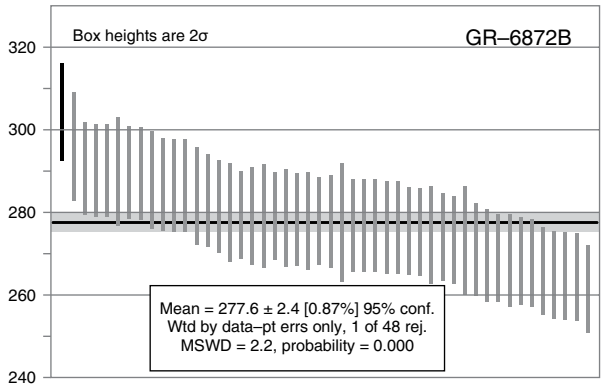
Box heights are 2σ
GR–6872B
Mean = 277.6 ± 2.4 [0.87%] 95% conf.
Wtd by data–pt errs only, 1 of 48 rej.
MSWD = 2.2, probability = 0.000

and edges, suggesting the occurrence of inherited antecrysts with ages from 300.1 ± 7.5 Ma to 292.1 ± 9.3 Ma. The ages of the principal group of zircons range from ca. 290 to 265 Ma, yielding a mean age of 280.1 ± 2.0 Ma (Figure 12) and a MSWD of 1.9, likely indicating the crystallization age of the rock. Spots with ages between 298 and 265 Ma show Th/U ratios ranging from 0.28 to 0.75, corroborating the igneous origin of the zircons.

Sample GOE–1098 presents stubby, prismatic, short–prismatic, and sub–spherical zircons. Under CL, most crystals show concentric zoning patterns, and a few inherited cores are truncated by external zoning or inherited cores of homogeneous texture (Figure 11). Of the 48 analyses, 2 were disregarded from the interpretation because these showed discordances higher than 10%. Seven inherited Carboniferous xenocrysts were identified (Table 6), presenting Th/U ratios ranging from 0.36 to 0.96. Three crystals with ages between 293–292 Ma and a Th/U ratio of 0.58–0.72 likely represent antecrysts. The remaining 27 ages vary between 289 and 269 Ma, with a Th/U ratio ranging from 0.39 to 1.04. These data yield a mean age of 280.5 ± 2.3 Ma and an MSWD of 2.2 (Figure 12), which is interpreted as the rock crystallization age.

In GR–6872B, the zircons are stubby and sub–spherical, with a maximum dimension of 100 μm. Under CL, crystals show homogeneous and irregular textures and few concentric zoning patterns (Figure 11). Results with discordances higher than 8%, inverse discordances lower than –5%, and $^{206}Pb/^{238}U$ ratio errors higher than 9% were disregarded during interpretation. One zircon, despite meeting the aforementioned criteria, yielded an age of ca. 140 Ma. This age was discarded because its geological meaning is unknown. A mean age of 277.6 ± 2.4 Ma with a MSWD of 2.2 and Th/U ratios ranging from 0.14 to 1.06 was obtained from 47 crystals (Figure 12). One crystal yielded a Carboniferous age (Table 6), likely corresponding to an inherited zircon.

Sample AMC–0185 shows short, prismatic zircon crystals of up to 80 × 120 μm. Under CL, two populations are differentiated: one consists of zoned crystals with homogenous cores and concentrically zoned rims, and the second encompasses crystals with zoned, inherited cores that are equivalent to the first population described, with overgrowths, which may be zoned or homogeneous (Figure 13). Nine of the 62 analyses were disregarded during interpretation because of discordances or uncertainties higher than 5%. Population 1, defined by 24 crystals with ages ranging from 363 to 309 Ma (Th/U ranging from 0.36 to 1.02), is interpreted as inheritance from Devonian – Carboniferous boundary and early – late Carboniferous rocks. Population 2 comprises zircons with ages ranging from 305.5 Ma to 262.5 Ma (n = 29 with Th/U ratio between 0.23 and 0.93). These zircons yielded a mean age of 293.8 ± 2.7 with a MSWD of 2.1 and are interpreted as the rock crystallization age.

Sample GOE–1096 contains prismatic zircons, most of which have large homogeneous cores and thin zoned mantles. Few crystals show truncation between cores and mantles or thick areas with concentric zoning (Figure 13). Results with discordances and uncertainties higher than 10% were disregarded. Sixty–one analyses with Th/U ratios ranging from 0.31 to 1.10 yielded ages between 303 and 262 Ma. Using the function "unmix ages" of Isoplot (Ludwig, 2012), three populations were determined as follows: (i) between ca. 306–287 Ma, yielding a mean age of 294.52 ± 1.6 Ma; (ii) between ca. 285–279 Ma, yielding a mean age of 284.3 ± 3.0 Ma; and (iii) between ca. 277–261 Ma, yielding a mean age of 274.0 ± 2.3 Ma and a MSWD of 1.04 likely corresponding to the crystallization age (Figure 14). An inherited Neoproterozoic crystal and four Carboniferous crystals were also obtained (Table 6).

Sample JPZ–010A shows prismatic zircons with bipyramidal terminations that under CL show concentric zoning with rare inherited cores (Figure 13). Results with discordances higher than 7% were disregarded during interpretation. Two datasets of inherited ages are identified as follows: the first consists of ages ranging from 312 to 307 Ma, and the second of ages from 286 to 281 Ma. Fifty–seven results with Th/U ratios ranging from 0.31 to 1.09 and ages ranging from 275 to 256 Ma yielded a mean age of 264.7 ± 1.2 Ma with a MSWD of 1.8 (Figure 14), which is interpreted as the rock crystallization age.

Sample AMC–0159A contains prismatic zircons with maximal dimensions ranging from 100 to 300 μm. Concentric zoning is identified in some cases (Figure 13). In total, 35 analyses were performed and the results with a discordance higher than 10% were disregarded. The Th/U ratios range from 0.54 to 1.24, typical of igneous zircons, and the ages range from 286 to 268 Ma. The group of 31 data yielded a mean of 274.9 ± 1.4 Ma with a MSWD of 0.96 (Figure 15), which is interpreted as the igneous rock crystallization age.

Sample MGOQ–008 shows prismatic euhedral zircons with bipyramidal terminations of up to 150 μm, many of which contain inclusions. Most zircons show concentric zoning under CL (Figure 13). Ten of the 40 analyses were disregarded because they had discordances higher than 10%. Four results correspond to inherited zircons: two of Proterozoic and two of Carboniferous age. Four ages between ca. 281–275 Ma could correspond to antecrysts. The other results ranged from 272 to 252 Ma, yielding a mean age of 262.7 ± 2.1 Ma and an MSWD of 1.6 (Figure 15). These data show Th/U ratios ranging from 0.44 to 1.55, typical of igneous zircons. The mean age corresponds to the rock crystallization age.

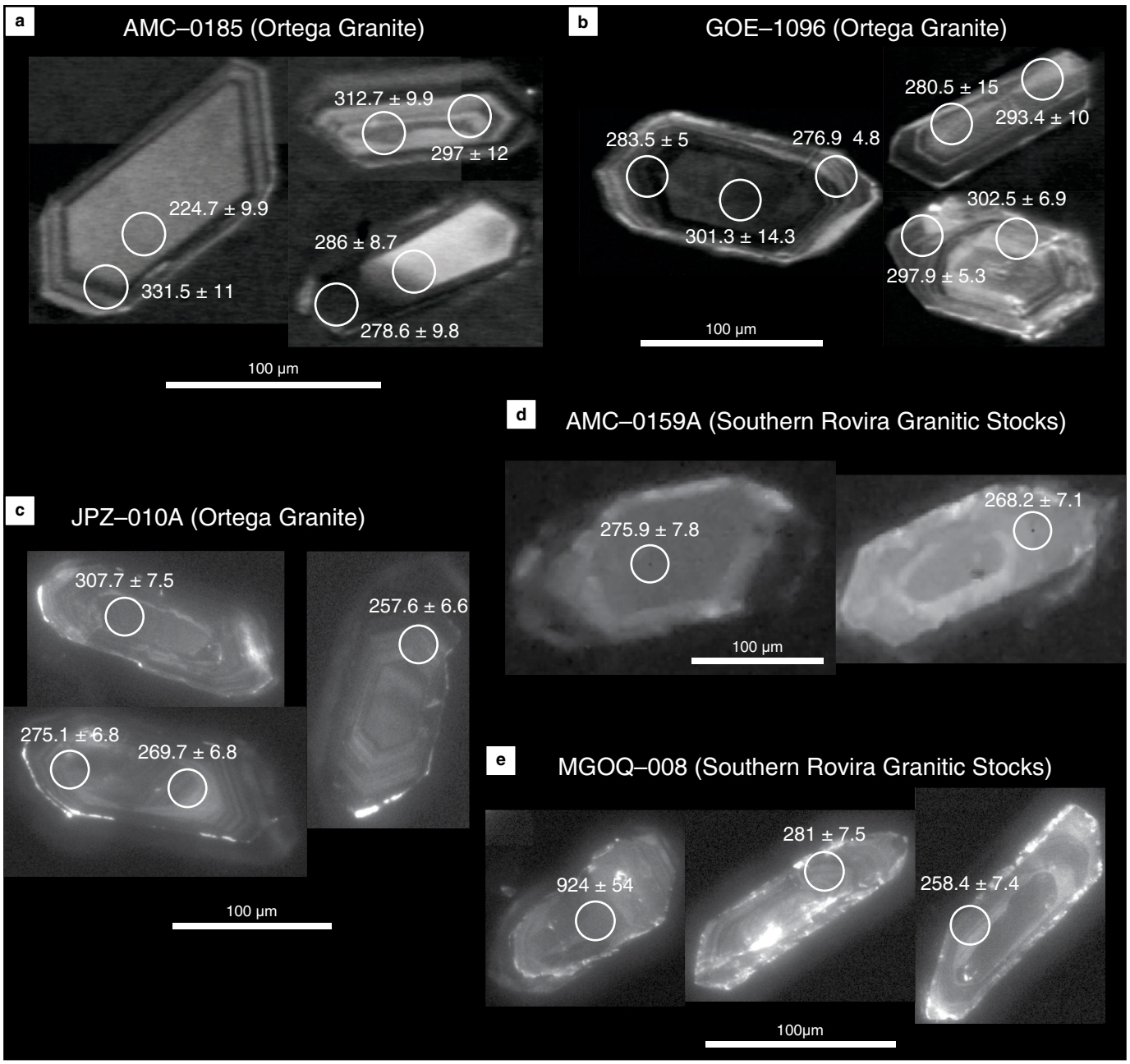

Figure 13. Cathodoluminescence images of representative zircons from samples: **(a)** AMC–0185, **(b)** GOE–1096, **(c)** JPZ–010A, **(d)** AMC–0159A, and **(e)** MGOQ–008.

7. Discussion and Conclusions

7.1. Characteristics of Permian Magmatism in Colombia

The composition of the Permian plutonic bodies in Colombia corresponds to quartz diorites, quartz monzonites, tonalites, granodiorites, monzogranites, and syenogranites (except for sample AMC–0159 of dacitic composition), including the rocks with migmatitic structures of La Plata Granite (Rodríguez et al., 2017) and granitoids within the Icarco Complex. In addition, some units show superimposed dynamic deformation, such as the Nechí Gneiss (Restrepo et al., 2011; Rodríguez et al., 2014) and El Encanto Orthogneiss (Cardona et al., 2010b; Piraquive, 2017), forming mylonites.

The geochemical data show that the Permian granitoids and gneisses are of calc–alkaline to high–K calc–alkaline character, varying from metaluminous to peraluminous, with negative Nb and Ti anomalies, and enrichment in Th and Nb. This suggests the input of recycled material from the crust during subduction processes (Pearce, 2008). The values of the (La/Yb)n versus Sr/Y ratios place these magmas in the field of continental arc magmas.

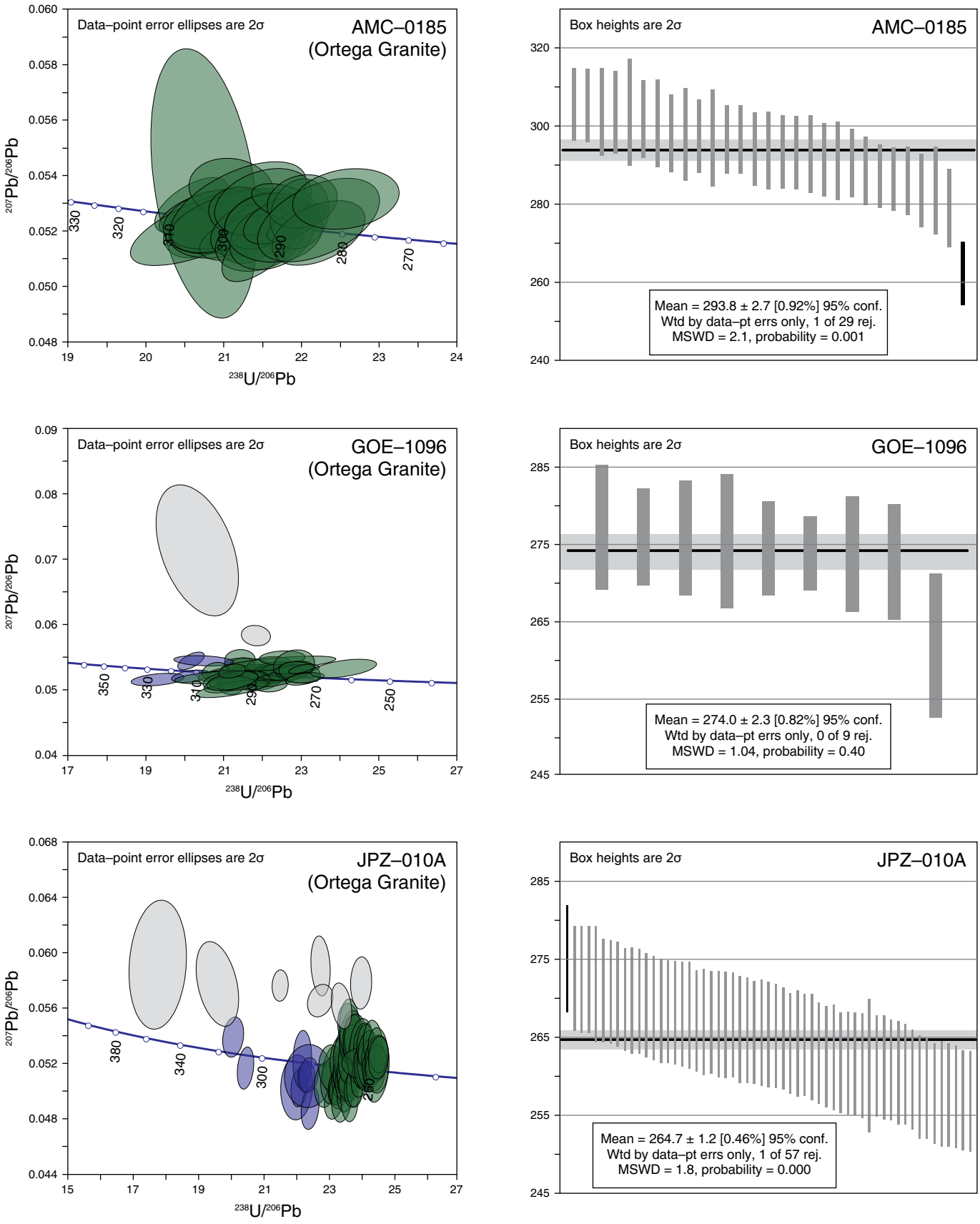

Figure 14. Tera–Wasserburg concordia diagrams and medians and/or means of Permian samples from the Ortega Granite. Gray ellipses: discarded results; blue ellipses: analysis in inherited zircons and anticrystals; green ellipses: Permian igneous ages.

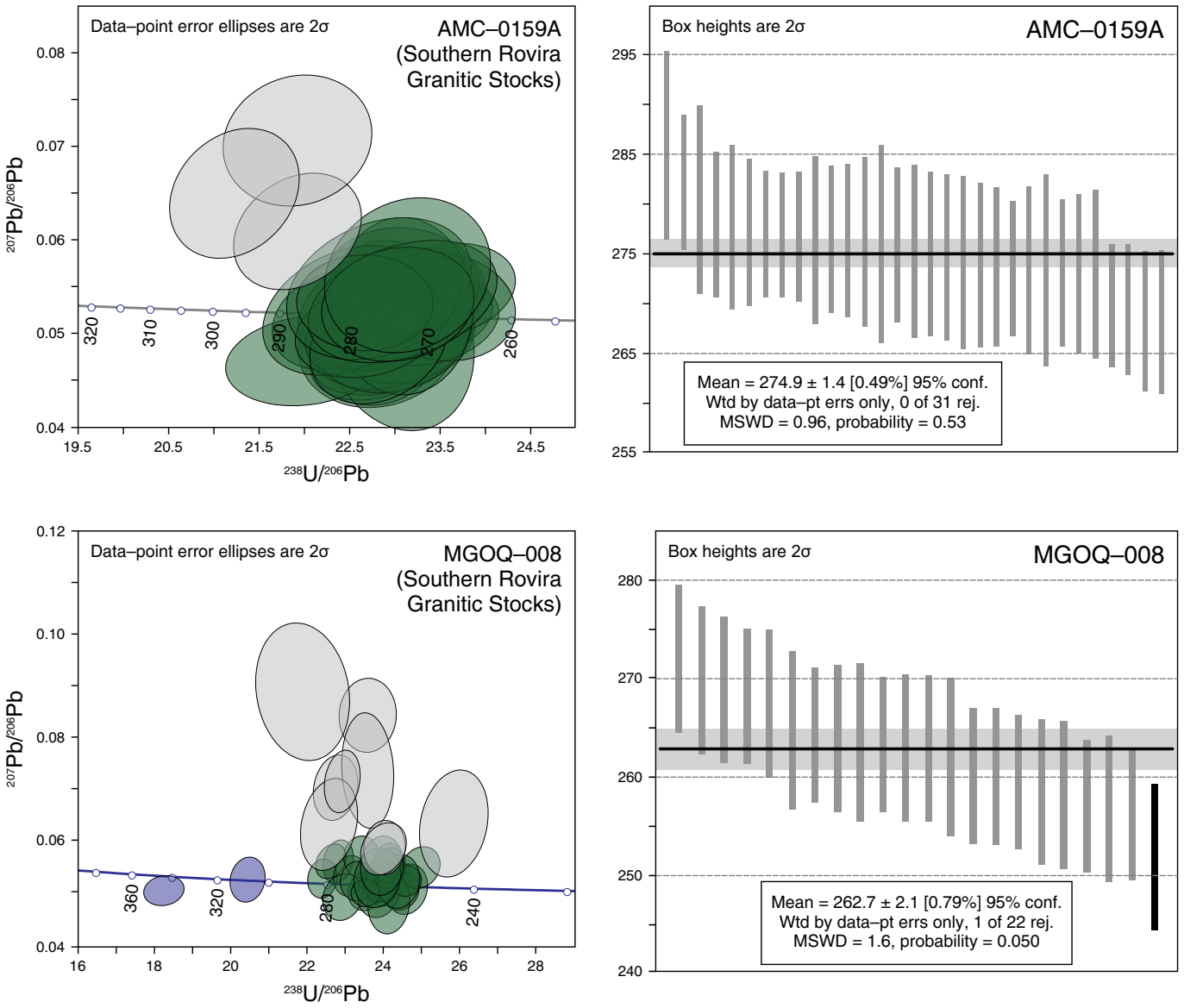

Figure 15. Tera–Wasserburg concordia diagrams and medians and/or means of samples from the southern Rovira Granitic Stocks. Gray ellipses: discarded results; blue ellipses: analysis of inherited zircons; green ellipses: Permian igneous ages.

The U–Pb Permian ages obtained in the granitoids are interpreted as pluton crystallization ages ranging from ca. 294 to 260 Ma. Figure 16 shows that during this period, several magmatic pulses occurred. In the Ortega Granite, ages range between ca. 294–290 Ma and ca. 283–263 Ma, presenting a major peak between 279–275 Ma. In El Encanto Orthogneiss, ages range from ca. 288 to 264 Ma. In an area near the serranía de San Lucas, ages range from ca. 281 to 263 Ma. In the southern Rovira Granitic Stocks ages range from ca. 275 to 263 Ma, and in La Plata Granite, ages range from ca. 278 to 268 Ma.

The inherited zircons yield Carboniferous and, to a lesser extent, Proterozoic, Cambrian, Ordovician, and Devonian ages (Figure 17a; Table 6). The few Proterozoic and Paleozoic inheritances (Figure 17b, xenocrysts) may suggest that the Permian arc locally assimilated the Neoproterozoic – Paleozoic basement. The Carboniferous inheritances are shown in Figure 17c.

Only two reports of magmatism during the Carboniferous have been published in Colombia. Leal–Mejía (2011) yielded igneous crystallization ages ranging from 333 to 310 Ma in diorites and tonalites of El Carmen Stock (west of the serranía de San Lucas on the northeastern slope of the Central Cordillera), and Silva–Arias et al. (2016) yielded an igneous crystallization age of 300 ± 1.3 Ma in a pyroxene gabbro in the Lower Magdalena Valley (Sitio Nuevo–1 well). Figure 17d shows that the Carboniferous inherited ages of the Permian units match the ages of the Carboniferous igneous occurrences known in Colombia.

The abundant Carboniferous inheritances (Th/U 0.34 to 1.02) in addition to the previous reports of Carboniferous units

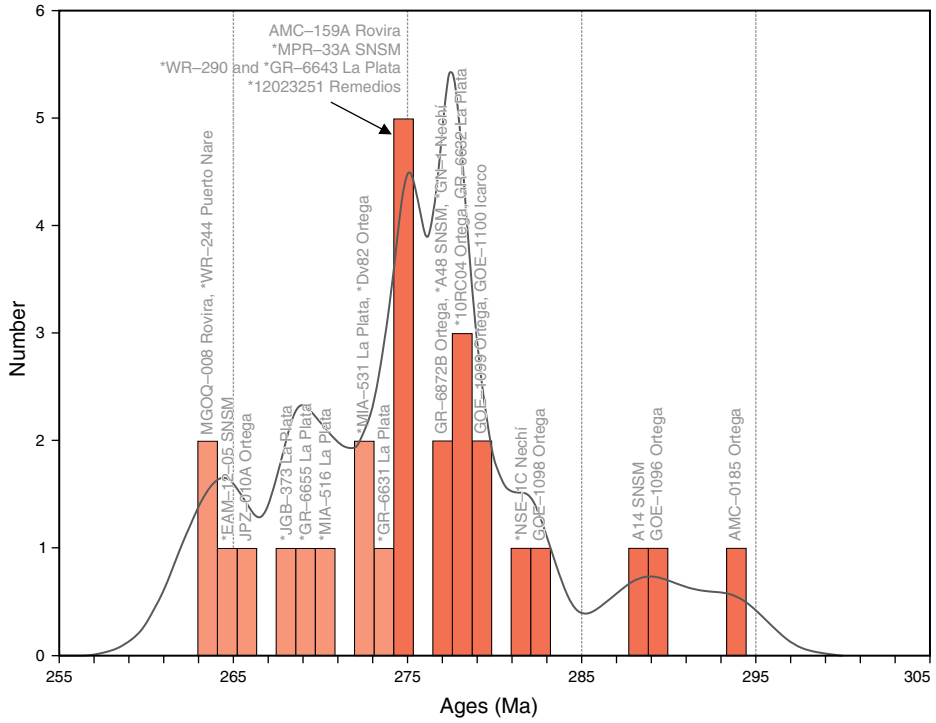

Figure 16. Probability density function of Permian igneous ages. Samples from other authors are preceded by an asterisk (*) (see Table 1 for references).

in Colombia (Figure 17c, 17d) suggest the existence of a larger arc that remains unidentified upon which the Permian arc was built, or that the magmatic activity began at the end of the Mississippian or the beginning of the Pennsylvanian (Figure 17c). This magmatism would have continued into the Permian, forming various plutonic bodies that crystallized during different pulses, similar to the Permian – Carboniferous arc of southwestern México (Ortega–Obregón et al., 2014).

7.2. Implications of the Metamorphism in Permian Rocks

The presence of metamorphic and plutonic rocks inside some units that comprise the Permian arc is difficult to explain and may be interpreted in several manners.

Although the structures and microtextures of La Plata Granite display metamorphic characteristics (see JGB–373A in Figure 18), all zircons yielded similar crystallization ages. These crystals are prismatic with concentric structures and Th/U ratios of approximately 1.0, without metamorphic overgrowths (Rodríguez et al., 2017). In addition, whole rock trace element and zircon geochemistry data indicate a geotectonic formation environment in a continental margin arc (Rodríguez et al., 2017). This suggests a tectonic environment in which the simultaneous formation of igneous and metamorphic rocks occurred.

Similarly, the granitoids of the Icarco Complex (Figures 2, 18) (Murillo et al., 1982) also exhibit metamorphic features. The analysis of a rock collected along the Río Blanco–Gaitán route (GOE–1100; crystallization age of 277.8 ± 2.1 Ma) presents slight mineral orientation, development of internal structures, and recrystallization resulting from thermal metamorphism (see GOE–1100 in Figure 18) likely caused by the intrusion of the Ibagué Batholith. Two Triassic concordant ages (ca. 245 Ma and ca. 223 Ma) obtained in the zircon cores of this sample show Th/U values of 0.76 and 0.22, suggesting an igneous origin for these crystals, and an additional age of ca. 242 Ma and a Th/U value of 0.14, which may reflect a metamorphic event. However, more data are required to validate this hypothesis.

We propose that La Plata Granite and the Icarco Complex blocks are part of the roots of the Permian arc.

The Nechí Gneiss, in contrast to the Permian bodies of the UMV, presents metamorphism following igneous crystallization. This unit outcrops west of the Neoproterozoic San Lucas Gneiss, and it is unknown if it is part of this basement or that of the Triassic metamorphic basement of the Central Cordillera (Restrepo et al., 2011) (Figure 3). According to Restrepo et al. (2011), U–Pb zircon ages of ca. 236 Ma suggest a Triassic metamorphic event that could be correlated with the metamorphism of the Tahamí Terrane. If so, these rocks would not be part of a Permian arc intruding the Neoproterozoic basement. On the other hand, we propose the possibility that the

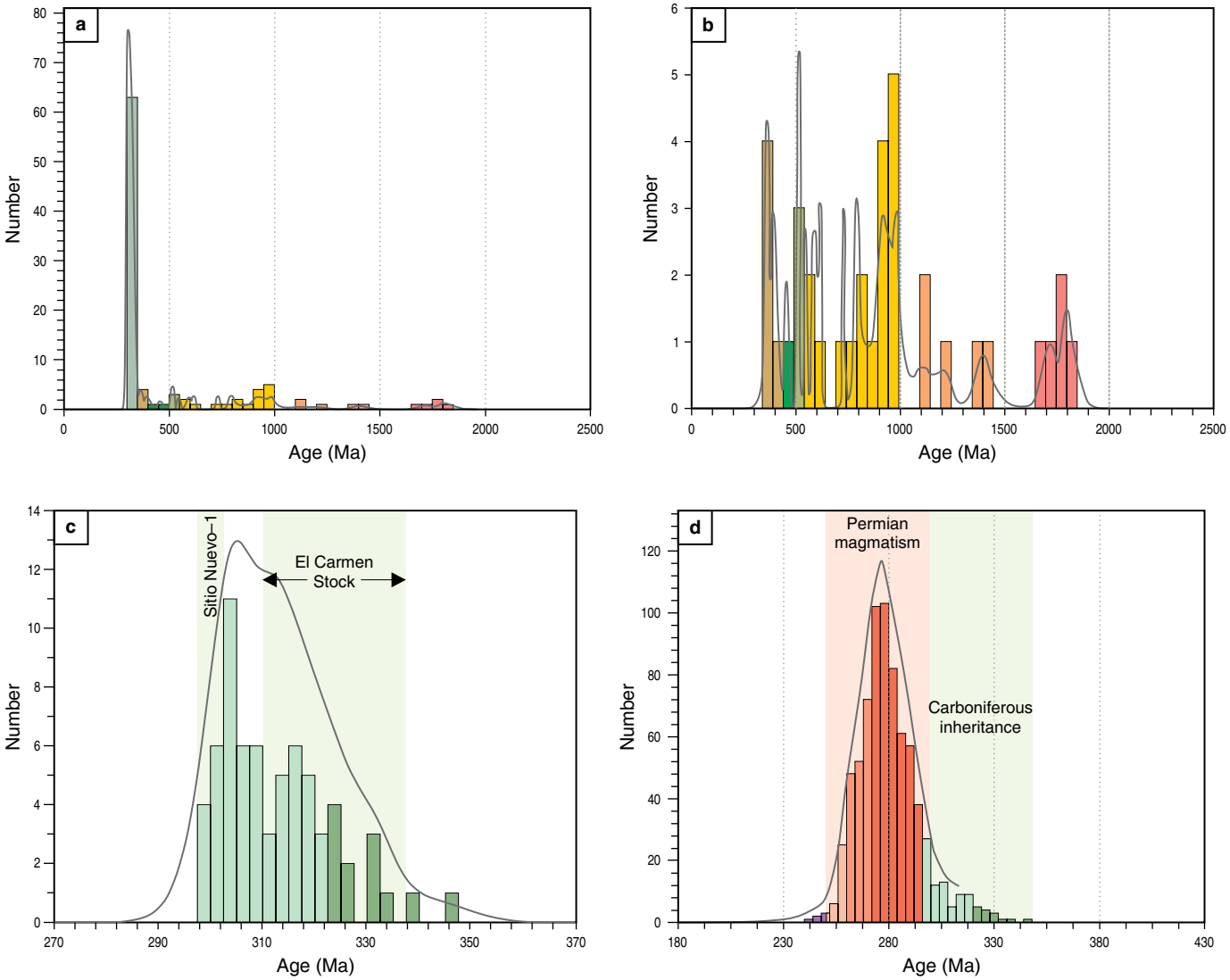

Figure 17. Relative probability diagrams with inheritances in the zircons from Permian rocks. **(a)** All inheritances from the Paleoproterozoic through the Carboniferous. **(b)** Detail of the inheritances between the Paleoproterozoic and the Devonian. **(c)** Probability diagram of the Carboniferous inheritances in Permian igneous rocks; the igneous age ranges of plutonic rocks from El Carmen Stock (Leal–Mejía, 2011) and the Sitio Nuevo–1 well (Silva–Arias et al., 2016) are indicated in fields highlighted in very light green. **(d)** Probability diagram of inherited and igneous ages of Permian rocks. Data sources: Cardona et al. (2010b), Rodríguez et al. (2017), Villagómez (2010), and this study.

ductile deformation characterizing this unit could be a result of the collision between the Neoproterozoic and Triassic basements during the Jurassic (Blanco–Quintero et al., 2014). In this case, the current position of the Nechí Gneiss would be tectonic in a Jurassic metamorphic block (hitherto inferred) and the age of metamorphism would be Late Jurassic. However, we still do not have an explanation for the Triassic metamorphic event.

The quartz–feldspar rocks of the Sierra Nevada de Santa Marta are mylonites and protomylonites (Cardona et al., 2010b; Piraquive, 2017) with Permian igneous crystallization ages and Neoproterozoic and Paleozoic inheritances, suggesting that these were emplaced in the Neoproterozoic basement (Cardona et al., 2010b). These bodies are tectonically along the western edge of the Neoproterozoic basement and inside Upper Jurassic metamorphic rocks. The ductile deformation and the development of metamorphic minerals are likely associated with collision between the Neoproterozoic (the Chibcha Terrane) and Triassic basements (the Tahamí Terrane) during the Late Jurassic.

7.3. Tectonic Implications and Correlations

Our results indicate that the Permian arc, previously reported in the SNSM (Cardona et al., 2010b) and the Central Cordillera (Cochrane et al., 2014; Leal–Mejía, 2011; Rodríguez et al., 2017; Villagómez, 2010), is more extensive and voluminous and includes parts of the SSL and UMV. This Permian magmatism may have peaked at the end of the Cisuralian, assimilating most rocks that originated during the previous stages of the arc

JGB–373A

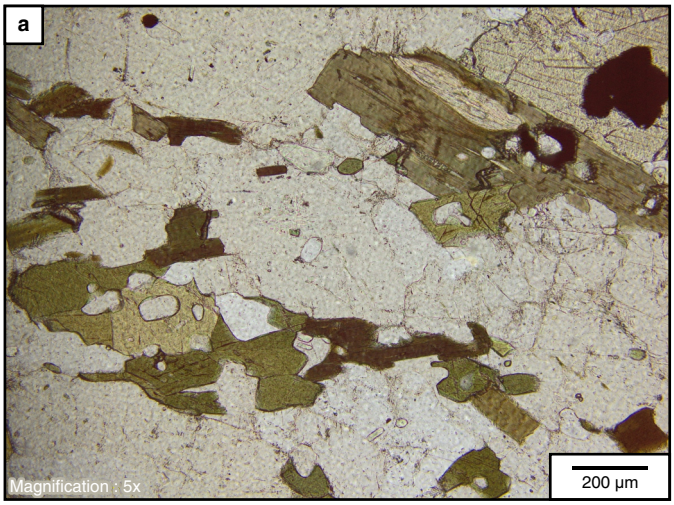

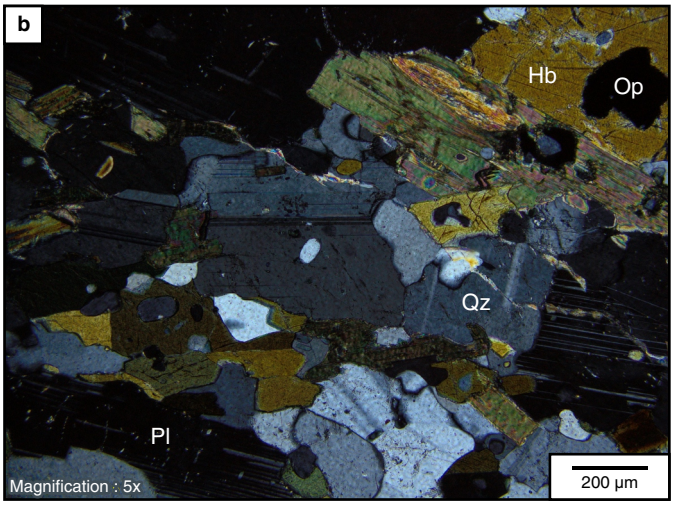

GOE–1100

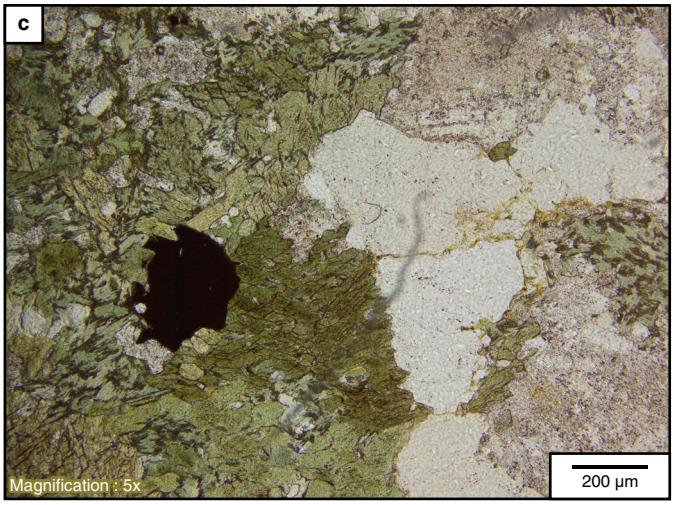

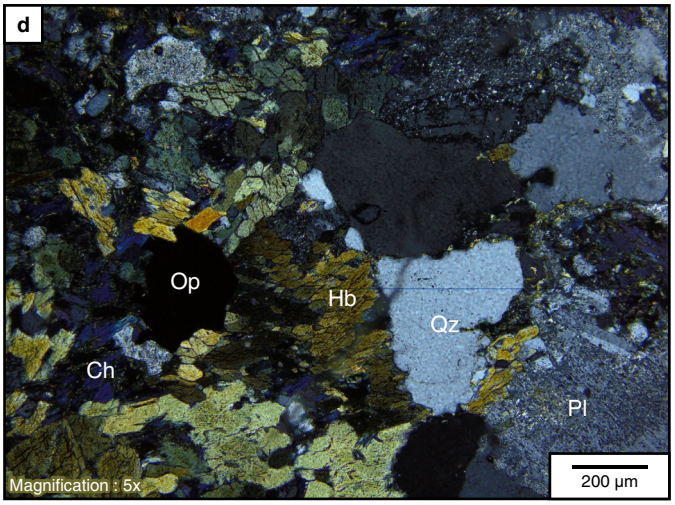

GZ–6678

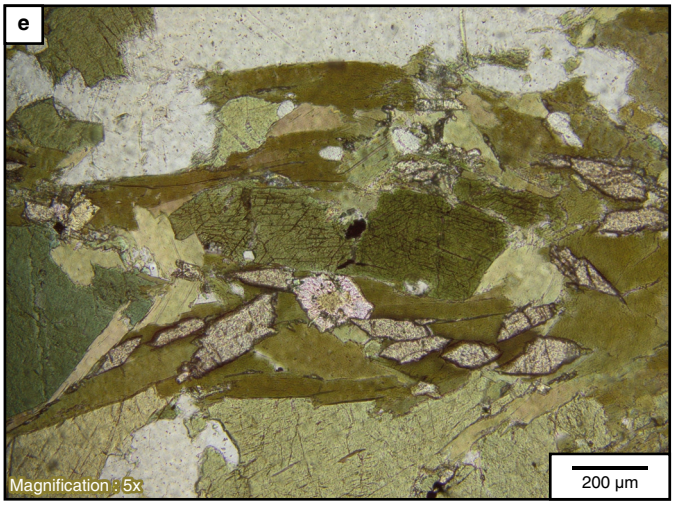

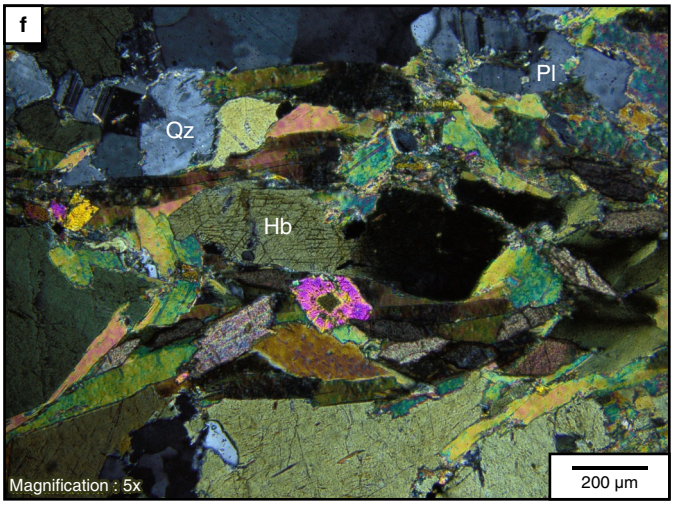

Figure 18. Microscopic aspect of metamorphic rocks of Permian age. **(a)** and **(b)** La Plata Granite (JGB–373A—granofels) granoblastic and granonematoblastic textures. **(c)** and **(d)** Icarco Complex (GOE–1100—meta–quartz diorite) recrystallization texture forming subgrains. **(e)** and **(f)** Nechí Gneiss (GZ–6678—gneisses) hornblende porphyroclasts and plagioclase and lepidoblastic metamorphic bands.

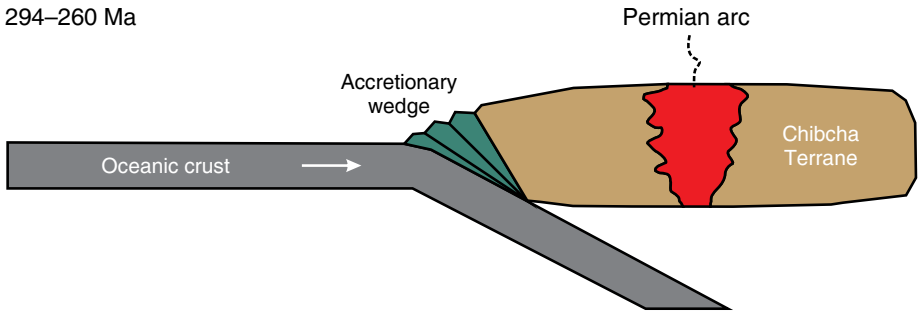

Figure 19. Tectonic model of a Permian arc on the western boundary of the Chibcha Terrane.

during the Carboniferous and the early Permian, intruding the Neoproterozoic basement of the Colombian Andes (Chibcha Terrane; Figure 19). Later, the arc was faulted in tectonic blocks together with the Early to Middle Jurassic arc.

The Permian arc rocks in Colombia are coeval with multiple plutonic units in Venezuela (serranía de Perijá sensu Dasch, 1982; El Baúl Massif sensu Viscarret et al., 2007, and Paraguaná Peninsula sensu van der Lelij et al., 2016); Ecuador (Paul et al., 2018); the Eastern Cordillera of Perú (Mišković et al., 2009); México (granitoids in the Chiapas and Mixtec Massifs sensu Weber & Köhler, 1999; Weber et al., 2005, 2007; and the Oaxaca and Acatlán Complexes sensu Ortega–Obregón et al., 2014).

In addition, their mineralogical and geochemical composition is consistent with rocks originating in a continental arc margin, as proposed by Cardona et al. (2010b). Vinasco et al. (2006) and Piraquive (2017), however, associate the genesis of the granitoids with the Ouachita–Alleghanian orogeny, caused by the Laurentia–Gondwana collision as a consequence of the closure of the Rheic Ocean during the Permian. Piraquive (2017) interprets the ages between 300–280 Ma as the result of collisional magmatism, while the ca. 278 Ma granitoids are post–collisional anatectic melts.

We suggest that the Permian arc originated in a subduction zone formed between the proto–Pacific Plate and the western margin of Pangea, coeval with the closure of the Rheic Ocean (Keppie et al., 2008; Nance et al., 2012). This arc was likely continuous from Perú to México and, as proposed by other authors, may have extended to the southern part of North America (Ortega–Obregón et al., 2014).

Acknowledgments

The authors express their gratitude to the Servicio Geológico Colombiano for their support in conducting the research project "Magmatismo Jurásico en Colombia" and to geologists Tomas CORREA, Lina María CETINA, Milton OBANDO, María Isabel GIRALDO, and Gilberto ZAPATA who aided in the sampling efforts. We would like to thank Diego RAMÍREZ for editing the text. Special thanks go to the staff of the Laser Ablation Geochronology Laboratory, Servicio Geológico Colombiano, including Jimmy Alejandro MUÑOZ, Cindy Lizeth URUEÑA, and Lorena del Pilar RAYO, for performing the U–Pb zircon dating and for acquiring luminescence images of the samples reported in this study.

References

Arango, M.I., Rodríguez, G., Zapata, G. & Bermúdez, J.G. 2015. Catálogo de unidades litoestratigráficas de Colombia: Monzogranito de Mocoa, cordillera Oriental, departamentos de Putumayo, Huila, Cauca y Nariño. Servicio Geológico Colombiano, 41 p. Bogotá.

Blanco–Quintero, I.F., García–Casco, A., Toro, L.M., Moreno–Sánchez, M., Ruiz, E.C., Vinasco, C.J., Cardona, A., Lázaro, C. & Morata, D. 2014. Late Jurassic terrane collision in the northwestern margin of Gondwana (Cajamarca Complex, eastern flank of the Central Cordillera, Colombia). International Geology Review, 56(15): 1852–1872. https://doi.org/10.1080/00206814.2014.963710

Bogotá, J. & Aluja, J. 1981. Geología de la serranía de San Lucas. Geología Norandina, (4): 49–55.

Botero, G. 1940. Geología sobre el Ordoviciano de Antioquia. Revista Minería, 17(99): 8249–8256.

Bustamante, C., Cardona, A., Saldarriaga, M., García–Casco, A., Valencia, V. & Weber, M. 2009. Metamorfismo de los esquistos verdes y anfibolitas pertenecientes a los Esquistos de Santa Marta, Sierra Nevada de Santa Marta (Colombia): ¿Registro de la colisión entre el arco del Caribe y la margen suramericana? Boletín de Ciencias de la Tierra, (25): 7–26.

Cárdenas, J., Fuquen, J. & Núñez, A. 1998. Geología de la plancha 388 Pitalito. Scale 1:100 000. Ingeominas. Bogotá.

Cardona, A., Chew, D., Valencia, V.A., Bayona, G., Mišković, A. & Ibañez–Mejia, M. 2010a. Grenvillian remnants in the northern Andes: Rodinian and Phanerozoic paleogeographic perspectives. Journal of South American Earth Sciences, 29(1): 92–104. https://doi.org/10.1016/j.jsames.2009.07.011

Cardona, A., Valencia, V., Garzón, A., Montes, C., Ojeda, G., Ruiz, J. & Weber, M. 2010b. Permian to Triassic I to S–type magmatic switch in the northeast Sierra Nevada de Santa Marta and adjacent regions, Colombian Caribbean: Tectonic setting and implications within Pangea paleogeography. Journal of South American Earth Sciences, 29(4): 772–783. https://doi.org/10.1016/j.jsames.2009.12.005

Carvajal, C., Fúquen, J.A. & Gómez, L.A. 1993. Geología de la plancha 282 Chaparral. Scale 1:100 000. Ingeominas. Ibagué.

Cediel, F., Mojica, J. & Macía, C. 1980. Definición estratigráfica del Triásico en Colombia, Suramérica. Formaciones Luisa, Payandé y Saldaña. Newsletters on Stratigraphy, 9(2): 73–104.

Chappell, B.W. & White, A.J.R. 1974. Two contrasting granite types. Pacific Geology, 8: 173–174.

Clavijo, J. 1995. Memoria explicativa: Mapa geológico de la plancha 75 Aguachica. Scale 1:100 000. Ingeominas, 48 p. Bucaramanga.

Cochrane, R.S. 2013. U–Pb thermochronology, geochronology and geochemistry of NW South America: Rift to drift transition, active margin dynamics and implications for the volume balance of continents. Doctorade thesis, University of Geneva, 118 p. Geneva. https://doi.org/10.13097/archive-ouverte/unige:30029

Cochrane, R., Spikings, R., Gerdes, A., Winkler, W., Ulianov, A., Mora, A. & Chiaradia, M. 2014. Distinguishing between in–situ and accretionary growth of continents along active margins. Lithos, 202–203: 382–394. https://doi.org/10.1016/j.lithos.2014.05.031

Condie, K.C. & Kröner, A. 2013. The building blocks of continental crust: Evidence for a major change in the tectonic setting of continental growth at the end of the Archean. Gondwana Research, 23(2): 394–402. https://doi.org/10.1016/j.gr.2011.09.011

Cuadros, F.A. 2012. Caracterização geoquímica e geocronológica do embasamento mesoproterozóico da parte norte da serranía de San Lucas (Colômbia). Master thesis, Universidade de Brasilia, 113 p. Brasilia.

Cuadros, F.A., Botelho, N.F., Ordóñez–Carmona, O. & Matteini, M. 2014. Mesoproterozoic crust in the San Lucas Range (Colombia): An insight into the crustal evolution of the northern Andes. Precambrian Research, 245: 186–206. https://doi.org/10.1016/j.precamres.2014.02.010

Dasch, L.E. 1982. U–Pb geochronology of the Sierra de Perijá, Venezuela. Master thesis, Case Western Reserve University, 183 p. Cleveland, USA.

Duque–Trujillo, J.F. 2009. Geocronología (U/Pb y $^{40}Ar/^{39}Ar$) y geoquímica de los intrusivos paleógenos de la Sierra Nevada de Santa Marta y sus relaciones con la tectónica del Caribe y el arco magmático circun–caribeño. Master thesis, Universidad Nacional Autónoma de México, 189 p. Queretaro, México.

Esquivel, J., Flores, D. & Núñez, A. 1991. Mapa geológico de la plancha 301 Planadas. Scale 1:100 000. Ingeominas. Ibagué.

Feininger, T., Barrero, D. & Castro, N. 1972. Geología de parte de los departamentos de Antioquia y Caldas (sub–zona II–B). Boletín Geológico, 20(2): 1–173.

Geyer, O.F. 1973. Das präkretazische Mesozoikum von Kolumbien. Geologisches Jahrbuch, 5: 1–155.

Gómez, J., Morales, C.J., Marquínez, G. & Velandia, F. 1999. Geología de la plancha 322 Santa María. Scale 1:100 000. Ingeominas. Bogotá.

Gómez, J., Montes, N.E., Nivia, Á. & Diederix, H., compilers. 2015. Geological Map of Colombia 2015. Scale 1:1 000 000. Servicio Geológico Colombiano, 2 sheets. Bogotá. https://doi.org/10.32685/10.143.2015.936.

Gómez, J., Montes, N.E., Alcárcel, F.A. & Ceballos, J.A. 2015b. Catálogo de dataciones radiométricas de Colombia en ArcGIS y Google Earth. In: Gómez, J. & Almanza, M.F. (editors), Compilando la geología de Colombia: Una visión a 2015. Servicio Geológico Colombiano, Publicaciones Geológicas Especiales 33, p. 63–419. Bogotá.

González, H. 2001. Memoria explicativa: Mapa geológico del departamento de Antioquia. Scale 1:400 000. Ingeominas, 240 p. Medellín.

Grosse, E. 1931. Acerca de la geología del sur de Colombia: Informe rendido al Ministerio de Industrias sobre un viaje al Huila y alto Caquetá. Boletín de Minas y Petróleo, IV, (23–24): 413–476.

Hubach, E. & Alvarado, B. 1932. Estudio geológico en la ruta Popayán–Bogotá. Servicio Geológico Nacional, Internal report 213, 133 p. Bogotá.

Ibañez–Mejia, M., Ruiz, J., Valencia, V.A., Cardona, A., Gehrels, G.E. & Mora, A. 2011. The Putumayo Orogen of Amazonia and its implications for Rodinia reconstructions: New U–Pb geochronological insights into the Proterozoic tectonic evolution of northwestern South America. Precambrian Research, 191(1–2): 58–77. https://doi.org/10.1016/j.precamres.2011.09.005

Ibañez–Mejia, M., Pullen, A., Arenstein, J., Gehrels, G., Valley, J., Ducea, M., Mora, A., Pecha, M. & Ruiz, J. 2015. Unraveling crustal growth and reworking processes in complex zircons from orogenic lower–crust: The Proterozoic Putumayo Orogen of Amazonia. Precambrian Research, 267: 285–310. https://doi.org/10.1016/j.precamres.2015.06.014

Irvine, T.N. & Baragar, W.R.A. 1971. A guide to the chemical classification of the common volcanic rocks. Canadian Journal of Earth Sciences, 8(5): 523–548. https://doi.org/10.1139/e71-055

Jiménez–Mejía, D.M., Juliani, C. & Cordani, U.G. 2006. P–T–t conditions of high–grade metamorphic rocks of the Garzón Massif,

Andean basement, SE Colombia. Journal of South American Earth Sciences, 21(4): 322–336. https://doi.org/10.1016/j.jsames.2006.07.001

Keppie, J.D., Dostal, J., Murphy, J.B. & Nance, R.D. 2008. Synthesis and tectonic interpretation of the westernmost Paleozoic Variscan orogen in southern Mexico: From rifted Rheic margin to active Pacific margin. Tectonophysics, 461(1–4): 277–290. https://doi.org/10.1016/j.tecto.2008.01.012

Kroonenberg, S. & Diederix, H. 1992. Geology of the uppermost Magdalena Valley, 21th Field Conference. In: Geotec Ltda. (editor), Geological field–trips: Colombia 1980–1989. Asociación Colombiana de Geólogos y Geofísicos del Petróleo, p. 73–89. Bogotá.

Leal–Mejía, H. 2011. Phanerozoic gold metallogeny in the Colombian Andes: A tectono–magmatic approach. Doctorade thesis, Universitat de Barcelona, 989 p. Barcelona.

Le Maitre, R.W., editor. 2002. Igneous rocks. A classification and glossary of terms. 2nd edition. Recommendations of the International Union of Geological Sciences Subcommission on the systematics of igneous rocks. Cambridge University Press, 236 p. New York, USA. https://doi.org/10.1017/CBO9780511535581

Ludwig, K.R. 2012. User's manual for Isoplot 3.75. A geochronological toolkit for Microsoft Excel. Berkeley Geochronology Center, Special Publication 5, 75 p. Berkeley, California.

Marshall, D.J. 1988. Cathodoluminescence of geological materials. Unwin Hyman, 146 p. London.

Martens, U., Restrepo, J.J., Ordoñez–Carmona, O. & Correa–Martínez, A.M. 2014. The Tahamí and Anacona Terranes of the Colombian Andes: Missing links between South American and Mexican Gondwana margins. The Journal of Geology, 122(5): 507–530. https://doi.org/10.1086/677177

Middlemost, E.A.K., 1994. Naming materials in the magma/igneous rock system. Earth–Science Reviews, 37(3–4): 215–224. https://doi.org/10.1016/0012-8252(94)90029-9

Miller, J.S., Matzel, J.E., Miller, C.F., Burgess, S.D. & Miller, R.B. 2007. Zircon growth and recycling during the assembly of large, composite arc plutons. Journal of Volcanology and Geothermal Research, 167(1–4): 282–299. https://doi.org/10.1016/j.jvolgeores.2007.04.019

Mišković, A., Spikings, R.A., Chew, D.M., Košler, J., Ulianov, A. & Schaltegger, U. 2009. Tectonomagmatic evolution of western Amazonia: Geochemical characterization and zircon U–Pb geochronologic constraints from the Peruvian eastern cordilleran granitoids. Geological Society of America Bulletin, 121(9–10): 1298–1324. https://doi.org/10.1130/B26488.1

Mojica, J. 1980. Observaciones acerca del estado actual del conocimiento de la Formación Payandé (Triásico Superior), valle superior del río Magdalena, Colombia. Geología Colombiana, (11): 67–88.

Mojica, J., Villarroel, C., Cuerda, A. & Alfaro, M.A. 1988. La fauna de graptolites de la Formación El Hígado (Llanvirniano?–Llandeiliano), serranía de Las Minas, Valle Superior del Magdalena, Colombia. V Congreso Geológico Chileno. Memoirs, II, p. 189–202. Santiago.

Montoya, J.C. & Ordóñez–Carmona, O. 2010. Cartografía geológica y caracterización petrográfica de las unidades litológicas asociadas a los cuerpos vetiformes de oro en el distrito minero Bagre–Nechí. Informe técnico, Grupo de Investigación en Georecursos, Minería y Medio Ambiente (GEMMA). Universidad Nacional de Colombia, 140 p. Medellín.

Mora, A., Ibañez–Mejia, M., Oncken, O., De Freitas, M., Vélez, V., Mesa, A. & Serna, L. 2017. Structure and age of the Lower Magdalena Valley Basin basement, northern Colombia: New reflection–seismic and U–Pb–Hf insights into the termination of the central Andes against the Caribbean Basin. Journal of South American Earth Sciences, 74: 1–26. https://doi.org/10.1016/j.jsames.2017.01.001

Mosquera, D., Núñez, A. & Vesga, C.J. 1982. Mapa geológico preliminar de la plancha 244 Ibagué. Scale 1:100 000. Ingeominas, 27 p. Bogotá.

Murillo, A., Esquivel, C. & Flores, D. 1982. Mapa geológico preliminar de la plancha 281 Rioblanco. Scale: 1:100 000. Ingeominas. Ibagué.

Nakamura, N. 1974. Determination of REE, Ba, Fe, Mg, Na and K in carbonaceous and ordinary chondrites. Geochimica et Cosmochimica Acta, 38(5): 757–775. https://doi.org/10.1016/0016-7037(74)90149-5

Nance, R.D., Gutiérrez–Alonso, G., Keppie, J.D., Linnemann, U., Murphy, J.B., Quesada, C., Strachan, R.A. & Woodcock, N.H. 2012. A brief history of the Rheic Ocean. Geoscience Frontiers, 3(2): 125–135. https://doi.org/10.1016/j.gsf.2011.11.008

Nelson, H.W. 1957. Contribution to the geology of the Central and Western Cordillera of Colombia in the sector between Ibagué and Cali. Leidse Geologische Mededelingen, 22: 1–75.

Núñez, A. & Murillo, A. 1982. Memoria explicativa: Geología y prospección geoquímica de las planchas 244 Ibagué y 263 Ortega. Ingeominas, Informe 1879, 388 p. Ibagué.

Núñez, A., Mosquera, D. & Vesga, C.J. 1984a. Geología de la plancha 263 Ortega. Scale 1:100 000. Ingeominas, 1 sheet. Bogotá.

Núñez, A., Mosquera, D. & Vesga, C.J. 1984b. Memoria explicativa: Mapa geológico preliminar de la plancha 263 Ortega. Scale 1:100 000. Ingeominas, 21 p. Bogotá.

Ordóñez–Carmona, O., Pimentel, M.M. & De Moraes, R. 2002. Granulitas de Los Mangos: Un fragmento grenvilliano en la parte oriental de la Sierra Nevada de Santa Marta. Revista de la Academia Colombiana de Ciencias Exactas, Físicas y Naturales, 26(99): 169–179.

Ordóñez–Carmona, O., Frantz, J.C., Chemale, F. & Londoño, C. 2009. Serranía de San Lucas: Mineralizaciones auríferas, intrusiones de 1500 Ma, metamorfismo Grenville y magmatismo Jurásico. XII Congreso Colombiano de Geología. Memoirs in CD ROM, T003–R117, 1 p. Paipa, Boyacá.

Ortega–Obregón, C., Solari, L., Gómez–Tuena, A., Elías–Herrera, M., Ortega–Gutiérrez, F. & Macías–Romo, C. 2014. Permian

– Carboniferous arc magmatism in southern Mexico: U–Pb dating, trace element and Hf isotopic evidence on zircons of earliest subduction beneath the western margin of Gondwana. International Journal of Earth Sciences, 103(5): 1287–1300. https://doi.org/10.1007/s00531-013-0933-1

Paul, A., Spikings, R., Ulianov, A. & Ovtcharova, M. 2018. High temperature (>350 °C) thermal histories of the long lived (>500 Ma) active margin of Ecuador and Colombia: Apatite, titanite and rutile U–Pb thermochronology. Geochimica et Cosmochimica Acta, 228: 275–300. https://doi.org/10.1016/j.gca.2018.02.033

Pearce, J.A. 2008. Geochemical fingerprinting of oceanic basalts with applications to ophiolite classification and the search for Archean oceanic crust. Lithos, 100(1–4): 14–48. https://doi.org/10.1016/j.lithos.2007.06.016

Peccerillo, A. & Taylor, S.R. 1976. Geochemistry of Eocene calc–alkaline volcanic rocks from the Kastamonu area, northern Turkey. Contributions to Mineralogy and Petrology, 58(1): 63–81. https://doi.org/10.1007/BF00384745

Piraquive, A. 2017. Structural framework, deformation and exhumation of the Santa Marta Schists: Accretion and deformational history of a Caribbean Terrane at the north of the Sierra Nevada de Santa Marta. Doctorade thesis, Université Grenoble Alpes and Universidad Nacional de Colombia, 393 p. Grenoble–Bogotá.

Restrepo, J.J. & Toussaint, J.F. 1989. Terrenos alóctonos en los Andes colombianos: Explicación de algunas paradojas geológicas. V Congreso Colombiano de Geología. Memoirs, I, p. 92–107. Bucaramanga.

Restrepo, J.J., Ordóñez–Carmona, O., Martens, U. & Correa–Martínez, A.M. 2009. Terrenos, complejos y provincias en la cordillera Central de Colombia. Ingeniería, Investigación y Desarrollo, 9(2): 49–56.

Restrepo, J.J., Ordóñez–Carmona, O., Armstrong, R. & Pimentel, M.M. 2011. Triassic metamorphism in the northern part of the Tahamí Terrane of the Central Cordillera of Colombia. Journal of South American Earth Sciences, 32(4): 497–507. https://doi.org/10.1016/j.jsames.2011.04.009

Rodríguez, G. 1995a. Petrografía del Macizo de La Plata, departamento del Huila. Revista Ingeominas, (5): 5–16.

Rodríguez, G. 1995b. Petrografía y microtexturas del Grupo Garzón y el Granito de Anatexis de El Recreo, Macizo de Garzón, cordillera Oriental, Colombia. Revista Ingeominas, (5): 17–36.

Rodríguez, G., Ferreira, P., Velandia, F. & Núñez, A. 1998. Geología de la plancha 366 Garzón. Scale 1:100 000. Ingeominas. Ibagué.

Rodríguez, G., Zapata, G., Velásquez, M.E., Cossio, U. & Londoño, A.C. 2003. Memoria explicativa: Geología de las planchas 367 Gigante, 368 San Vicente del Caguán, 389 Timaná, 390 Puerto Rico, 391 Lusitania (parte noroccidental) y 414 El Doncello. Scale 1:100 000. Ingeominas, 166 p. Bogotá.

Rodríguez, G., Arango, M.I., Zapata, G. & Bermúdez, J.G. 2014. Petrografía y geoquímica del Neis de Nechí. Boletín de Geología, 36(1): 71–84.

Rodríguez, G., Zapata, G., Arango, M.I. & Bermúdez, J.G. 2015. Catálogo de unidades litoestratigraficas de Colombia: Monzogranito de Algeciras. Servicio Geológico Colombiano, 37 p. Medellín.

Rodríguez, G., Arango, M., Zapata, G. & Bermúdez, J. 2016. Catálogo de unidades litoestratigráficas de Colombia: Formación Saldaña. Servicio Geológico Colombiano, 91 p. Medellín.

Rodríguez, G., Zapata, G., Arango, M.I. & Bermúdez, J.G. 2017. Caracterización petrográfica, geoquímica y geocronología de rocas granitoides pérmicas al occidente de La Plata y Pacarní, Huila, Valle Superior del Magdalena, Colombia. Boletín de Geología, 39(1): 41–68. https://doi.org/10.18273/revbol.v39n1-2017002

Rodríguez, G., Arango, M.I., Zapata, G. & Bermúdez, J.G. 2018. Petrotectonic characteristics, geochemistry and U–Pb geochronology of Jurassic plutons in the Upper Magdalena Valley, Colombia: Implications on the evolution of magmatic arcs in the NW Andes. Journal of South American Earth Sciences, 81: 10–30. https://doi.org/10.1016/j.jsames.2017.10.012

Royero, J.M. 1996. Memoria explicativa: Geología de la plancha 65 Tamalameque (departamentos de Cesar y Bolívar). Ingeominas, 78 p. Bucaramanga.

Rubatto, D. 2002. Zircon trace element geochemistry: Partitioning with garnet and the link between U–Pb ages and metamorphism. Chemical Geology, 184(1–2): 123–138. https://doi.org/10.1016/S0009-2541(01)00355-2

Schoene, B., Crowley, J.L., Condon, D.J., Schmitz, M.D. & Bowring, S.A. 2006. Reassessing the uranium decay constants for geochronology using ID–TIMS U–Pb data. Geochimica et Cosmochimica Acta, 70(2): 426–445. https://doi.org/10.1016/j.gca.2005.09.007

Shand, S.J. 1943. Eruptive rocks. Their genesis, composition, classification, and their relation to ore deposits, with a chapter on meteorites. Geological Magazine, 64(7): 329–330. https://doi.org/10.1017/S0016756800103504

Siégel, C., Bryan, S.E., Allen, C.M. & Gust, D.A. 2018. Use and abuse of zircon–based thermometers: A critical review and a recommended approach to identify antecrystic zircons. Earth–Science Reviews, 176: 87–116. https://doi.org/10.1016/j.earscirev.2017.08.011

Silva–Arias, A., Páez–Acuña, L.A., Rincón–Martínez, D., Tamara–Guevara, J.A., Gómez–Gutiérrez, P.D., López–Ramos, E., Restrepo–Acevedo, S.M., Mantilla–Figueroa, L.C. & Valencia, V. 2016. Basement characteristics in the Lower Magdalena Valley and the Sinú and San Jacinto fold belts: Evidence of a Late Cretaceous magmatic arc at the south of the Colombian Caribbean. Ciencia, Tecnología y Futuro, 6(4): 5–36.

Sláma, J., Košler, J., Condon, D.J., Crowley, J.L., Gerdes, A., Hanchar, J.M., Horstwood, M.S.A., Morris, G.A., Nasdala, L.,

Norberg, N., Schaltegger, U., Schoene, B., Tubrett, M.N. & Whitehouse, M.J. 2008. Plešovice zircon–A new natural reference material for U–Pb and Hf isotopic microanalysis. Chemical Geology, 249(1–2): 1–35. https://doi.org/10.1016/j.chemgeo.2007.11.005

Solari, L., Gómez–Tuena, A., Bernal, J., Pérez–Arvizu, O. & Tanner, M. 2010. U–Pb zircon geochronology with an integrated LA–ICP–MS microanalytical workstation: Achievements in precision and accuracy. Geostandards and Geoanalytical Research, 34(1): 5–18. https://doi.org/10.1111/j.1751-908X.2009.00027.x

Spikings, R., Cochrane, R., Villagómez, D., van der Lelij, R., Vallejo, C., Winkler, W. & Beate, B. 2015. The geological history of northwestern South America: From Pangaea to the early collision of the Caribbean Large Igneous Province (290–75 Ma). Gondwana Research, 27(1): 95–139. https://doi.org/10.1016/j.gr.2014.06.004

Stacey, J.S. & Kramers, J.D. 1975. Approximation of terrestrial lead isotope evolution by a two–stage model. Earth and Planetary Science Letters, 26(2): 207–221. https://doi.org/10.1016/0012-821X(75)90088-6

Stibane, F. & Forero, A. 1969. Los afloramientos del Paleozoico en La Jagua (Huila) y río Nevado (Santander del sur). Geología Colombiana, (6): 31–66.

Streckeisen, A. 1974. Classification and nomenclature of plutonic rocks recommendations of the IUGS subcommission on the systematics of igneous rocks. Geologische Rundschau, 63(2): 773–786. https://doi.org/10.1007/BF01820841

Streckeisen, A. 1979. Classification and nomenclature of volcanic rocks, lamprophyres, carbonatites, and melilitic rocks: Recommendations and suggestions of the IUGS subcommission on the systematics of igneous rocks. Geology, 7(7): 331–335. https://doi.org/10.1130/0091-7613(1979)7<331:CANOVR>2.0.CO;2

Sun, S.S. & McDonough, W.F. 1989. Chemical and isotopic systematics of oceanic basalts: Implications for mantle composition and processes. In: Saunders, A.D. & Norry, M.J. (editors), Magmatism in the ocean basins. Geological Society of London, Special Publication 42, p. 313–345. https://doi.org/10.1144/GSL.SP.1989.042.01.19

Tschanz, C.M., Jimeno, A. & Cruz, J. 1969. Mapa geológico de reconocimiento de la Sierra Nevada de Santa Marta. Scale 1:200 000. Ingeominas. Bogotá.

Tschanz, C.M., Marvin, R.F., Cruz, J., Mehnert, H.H. & Cebula, G.T. 1974. Geologic evolution of the Sierra Nevada de Santa Marta, northeastern Colombia. Geological Society of America Bulletin, 85(2): 273–284. https://doi.org/10.1130/0016-7606(1974)85<273:GEOTSN>2.0.CO;2

van der Lelij, R., Spikings, R., Ulianov, A., Chiaradia, M. & Mora, A. 2016. Palaeozoic to Early Jurassic history of the northwestern corner of Gondwana, and implications for the evolution of the Iapetus, Rheic and Pacific Oceans. Gondwana Research, 31: 271–294. https://doi.org/10.1016/j.gr.2015.01.011

Velandia, F., Ferreira, P., Rodríguez, G. & Núñez, A. 1996. Levantamiento geológico de la plancha 366 Garzón, Huila. Ingeominas, Internal report 2321, 121 p. Ibagué.

Velandia, F., Morales, C.J, Caicedo, J.C. & Núñez, A. 1999. Geología de la plancha 345 Campoalegre. Scale 1:100 000. Ingeominas. Ibagué.

Velandia, F., Ferreira, P., Rodríguez, G. & Núñez, A. 2001a. Memoria explicativa: Levantamiento geológico de la plancha 366 Garzón. Ingeominas, 82 p. Bogotá.

Velandia, F., Nuñez, A. & Marquínez, G. 2001b. Memoria explicativa: Mapa geológico departamento del Huila. Scale 1:300 000. Ingeominas, 151 p. Bogotá.

Vesga, C.J. & Barrero, D. 1978. Edades K/Ar en rocas ígneas y metamórficas de la cordillera Central de Colombia y su implicación geológica. II Congreso Colombiano de Geología. Abstracts, p. 19. Bogotá.

Villagómez, D.R. 2010. Thermochronology, geochronology and geochemistry of the Western and Central Cordilleras and Sierra Nevada de Santa Marta, Colombia: The tectonic evolution of NW South America. Doctorade thesis, University of Geneva, 143 p. Geneva. https://doi.org/10.13097/archive-ouverte/unige:14270

Villarroel, C. & Mojica, J. 1988. El Paleozoico superior (Carbonífero–Pérmico) sedimentario de Colombia. Afloramientos conocidos y características generales. Geología Colombiana, (16): 81–87.

Vinasco, C.J., Cordani, U.G., González, H., Weber, M. & Peláez, C. 2006. Geochronological, isotopic, and geochemical data from Permo–Triassic granitic gneisses and granitoids of the Colombian central Andes. Journal of South American Earth Sciences, 21(4): 355–371. https://doi.org/10.1016/j.jsames.2006.07.007

Viscarret, P., Wright, J. & Urbani, F. 2007. Dataciones U/Pb SHRIMP en circón de rocas del Macizo El Baúl, estado Cojedes, Venezuela. IX Congreso Geológico Venezolano. Memoirs in CD ROM, p. 94–95. Caracas.

Weber, B. & Köhler, H. 1999. Sm–Nd, Rb–Sr and U–Pb geochronology of a Grenville Terrane in southern Mexico: Origin and geologic history of the Guichicovi Complex. Precambrian Research, 96(3–4): 245–262. https://doi.org/10.1016/S0301-9268(99)00012-1

Weber, B., Cameron, K.L., Osorio, M. & Schaaf, P. 2005. A late Permian tectonothermal event in Grenville crust of the southern Maya Terrane: U–Pb zircon ages from the Chiapas Massif, southeastern Mexico. International Geology Review, 47(5): 509–529. https://doi.org/10.2747/0020-6814.47.5.509

Weber, B., Iriondo, A., Premo, W.R., Hecht, L. & Schaaf, P. 2007. New insights into the history and origin of the southern Maya Block, SE México: U–Pb–SHRIMP zircon geochronology from metamorphic rocks of the Chiapas Massif. International Journal of Earth Sciences, 96(2): 253–269. https://doi.org/10.1007/s00531-006-0093-7

Wiedenbeck, M., Allé, P., Corfu, F., Griffin, W.L., Meier, M., Oberli, F., von Quadt, A., Roddick, J.C. & Spiegel, W. 1995. Three natural

zircon standards for U–Th–Pb, Lu–Hf, trace element and REE analyses. Geostandards and Geoanalytical Research, 19(1): 1–23. https://doi.org/10.1111/j.1751-908X.1995.tb00147.x

Zapata, G., Rodríguez, G., Arango, M.I. & Bermúdez, J.G. 2015. Catálogo de unidades litoestratigráficas de Colombia: Cuarzomonzodiorita de Páez, cordillera Central, Cauca–Huila. Servicio Geológico Colombiano, 50 p. Bogotá.

Zuluaga, C.A. & Stowell, H. 2012. Late Cretaceous – Paleocene metamorphic evolution of the Sierra Nevada de Santa Marta: Implications for Caribbean geodynamic evolution. Journal of South American Earth Sciences, 34: (1–9). https://doi.org/10.1016/j.jsames.2011.10.001

Explanation of Acronyms, Abbreviations, and Symbols:

CL	Cathodoluminescence
EDS	Energy dispersive X–ray spectroscopy
HFSE	High field strength element
ICP–MS	Inductively coupled plasma mass spectrometry
LA–ICP–MS	Laser ablation inductively coupled plasma mass spectrometry
LILE	Large–ion lithophile element
LOI	Loss on ignition
REE	Rare earth element
SGC	Servicio Geológico Colombiano
SNSM	Sierra Nevada de Santa Marta
SGC	Servicio Geológico Colombiano
SSL	Serranía de San Lucas
UMV	Upper Magdalena Valley
UNAM	Universidad Nacional Autónoma de México

Authors' Biographical Notes

Gabriel RODRÍGUEZ–GARCÍA graduated in 1987 with a degree in geological engineering from the Universidad Nacional de Colombia, Sede Medellín. Subsequently, he completed specialization studies at the École Nationale Supérieure des Mines de Paris in 1995, specializing in technical evaluation–economics of mining projects. He has worked for 30 years at the Servicio Geológico Colombiano. He was the head of cartography of the regional headquarters of Ibagué, and acts as coordinator of projects and regional cartography and of work groups for the exploration and evaluation of deposits. He currently coordinates the Medellín headquarters and the Grupo de Estudios Geológicos Especiales of the Servicio Geológico Colombiano. He has previously been a professor of Colombian Geology, Field Geology I, and Physical Geology at Universidad EAFIT and the director of geology of Grupo Argos. He has authored over 100 publications, including geological maps, memoirs, and scientific articles in geology.

Ana María CORREA–MARTÍNEZ graduated in geological engineering from the Universidad Nacional de Colombia, Sede Medellín and has a PhD in geology from the Universidade de Brasília (Brasil), where she studied the petrogenesis of the Aburrá Ophiolite in the Colombian Central Cordillera. Between 2008 and 2013, she worked as a gold exploration geologist and chief of mineral exploration projects. She was lecturer at the Universidad Nacional de Colombia (Medellín) in the Departamento de Recursos Minerales. Since 2014, she has worked in the Servicio Geológico Colombiano on geochronology of metamorphic units from the northwestern slope of the Central Cordillera and on the project "Jurassic Magmatism in the Colombian Andes".

Juan Pablo ZAPATA–VILLADA is a geological engineer and MS in mineral resources of Universidad Nacional de Colombia Sede Medellín. He worked for the Cordilleran project of México (Tectonic Analysis), and has expertise in GIS, U–Pb analysis, and heavy minerals. He works for the Servicio Geológico Colombiano. His job includes GIS and the geochronology, and geochemistry of the Western Cordillera and Jurassic magmatism in Colombia. He has participated as a speaker at the Colombian Geological Congress, winning the Ricardo Lleras Codazzi in the XIV edition.

Gloria OBANDO–ERAZO has a BS in geology, Universidad Nacional de Colombia Sede Bogotá, an MS in environmental geology with an emphasis in geophysics, processing and interpretation of aerial gamma ray spectrometry and aerial magnetometry (Universidade de Brasília, 2001), and is a PhD candidate in aerial geophysics (Universidade de Brasilia, 2006). She has worked since 1995 on multiple projects in Colombia using potential fields at the Servicio Geológico Colombiano. Since 2014, she has been working in the Grupo de Estudios Geológicos Especiales of the Servicio Geológico Colombiano on the project "Jurassic Magmatism in the Colombian Andes".

Bogotá, Colombia
2020